Advances in Experimental Mechanics VIII

Edited by
R. L. Burguete, M. Lucas, E. A. Patterson, S. Quinn

TTP TRANS TECH PUBLICATIONS

Advances in Experimental Mechanics VIII

Edited by
R.L. Burguete
M. Lucas
E.A. Patterson
S.Quinn

Advances in Experimental Mechanics VIII

Selected, peer-reviewed papers of the
8th International Conference on
Advances in Experimental Mechanics: Integrating Simulation and Experimentation for Validation,
(BSSM 2011)
Sept.7-9 2011, Edinburgh, Scotland

Edited by

R. L. Burguete
Airbus

M. Lucas
University of Glasgow

E. A. Patterson
Michigan State University

S. Quinn
University of Southampton

Trans Tech Publications Ltd
Kreuzstrasse 10
CH-8635 Durnten-Zurich
Switzerland
http://www.ttp.net

Volume 70 of
Applied Mechanics and Materials
ISSN 1660-9336

Full text available online at http://www.scientific.net

Distributed worldwide by

Trans Tech Publications Ltd
Kreuzstrasse 10
CH-8635 Durnten-Zuerich
Switzerland

Fax: +41 (44) 922 10 33
e-mail: sales@ttp.net

and in the Americas by

Trans Tech Publications Inc.
PO Box 699, May Street
Enfield, NH 03748
USA

Phone: +1 (603) 632-7377
Fax: +1 (603) 632-5611
e-mail: sales-usa@ttp.net

PREFACE

This volume of Applied Mechanics and Materials contains the papers presented at the joint 2011 Annual British Society for Strain Measurement Conference and the 2011 Fall Society for Experimental Mechanics Conference. This is the first time that the two societies have organised their conferences together. However, it is the sixth time that the papers from an Annual British Society for Strain Measurement Conference have been published as a collection in a volume of Applied Mechanics and Materials. The 82 papers in this volume represent the diverse nature of Experimental Mechanics with a focus on Integrating Simulation and Experimentation for Validation. The papers come from both academia and industry with more than half the contributions coming from outside the UK, reflecting the international nature of this event. We thank the authors and the referees for their hard work and dedication in the preparation and review of the papers.

We thank the organising committee and in particular, Paul Manning and Biana Gale, of the BSSM, for their effort and support in helping us compile this volume.

Richard Burguete, Airbus
Margaret Lucas, University of Glasgow
Eann Patterson, Michigan State University
Simon Quinn, University of Southampton

May 2011

BRITISH SOCIETY FOR STRAIN MEASUREMENT

Organising Committee

Richard **Burguete**	Airbus	UK
Biana **Gale**	BSSM	UK
Margaret **Lucas** (Conference Co-Chair)	University of Glasgow	UK
Paul **Manning**	BSSM	UK
Eann **Patterson** (Conference Co-Chair)	Michigan State University	USA
Simon **Quinn**	University of Southampton	UK
Wei-Chung **Wang**	National Tsinghua University	Taiwan
Kristin **Zimmerman**	General Motors Corporation	USA

Scientific Committee

Prof. Anand **Asundi**	Nanyang Technological University	Singapore
Prof. Douglas **Adams**	Purdue University	USA
Prof. Janice **Barton**	University of Southampton	UK
Dr. Eric **Brown**	Los Alamos National Laboratory	USA
Dr. John A. **Cafeo**	General Motors	USA
Prof. Terry **Chen**	National Cheng Kung University	Taiwan
Prof. Jaime **Domínguez**	University of Seville	Spain
Prof. Josef **Eberhardsteiner**	Vienna University of Technology	Austria
Prof. Jose **Freire**	Pontifical Catholic University of Rio de Janeiro	Brazil
Prof. Shan **Fu**	Shanghai Jaio Tong University	China
Prof. Emmanuel **Gdoutos**	Democritus University of Thrace	Greece
Prof. Michel **Grediac**	Blaise Pascal University	France
Dr. Erwin **Hack**	EMPA	Switzerland
Prof. Xiaoyuan **He**	Southeast University, Nanjing	China
Prof. Jon **Huntley**	Loughborough University	UK
Prof. Peter **Ifju**	University of Florida	USA
Prof. Daniel J. **Inman**	Virginia Polytechnic Institute & State University	USA

Sponsors

Airbus

AMEC Power and Process Europe

AWE

Doosan Babcock

GOM

Imetrum

LAVision

Photron

Stresstech Group

Co-Sponsors

Asian Society of Experimental Mechanics

Association Française de Mécanique

Canadian Society for Mechanical Engineering

Engineering Integrity Society

www.e-i-s.org.uk

Forum for Applied Mechanics

The British Institute of Non-destructive Testing

European Association for Experimental Mechanics

UK Forum for Engineering Structural Integrity

German Society for Experimental Stress Analysis

Institution of Mechanical Engineers

Institute of Physics - Applied Mechanics Group

Japanese Society for Experimental Mechanics

NAFEMS

Italian Association for Stress Analysis

Table of Contents

Session 5a: Material Behaviour

Session 5b: Measurement Innovations

Session 6a: Residual Stress

Session 6b: Vibration Analysis

Session 7: Validation Methods

Session 8a: Damage in Composite Materials

Session 8b: Thermal Deformation

Session 9a: Photoelasticity

Session 9a: Thermomechanics

Applied Mechanics and Materials Vol. 70 (2011) pp 1-20
© (2011) Trans Tech Publications, Switzerland
doi:10.4028/www.scientific.net/AMM.70.1

What Optical Metrology can do for Experimental Mechanics?

Wolfgang Osten

Institut für Technische Optik, Universität Stuttgart,

Pfaffenwaldring 9, D-70569 Stuttgart, Germany

osten@ito.uni-stuttgart.de

Keywords: optical metrology, digital mage processing, experimental stress analysis, non-destructive testing, material parameters, calibration, remote metrology, remote laboratories.

Abstract. Optical metrology has shown to be a versatile tool for the solution of many measurement and inspection problems. The main advantages of optical methods are the non-contact nature, the non-destructive and areal working principle, the fast response, high sensitivity, resolution and accuracy. Consequently, optical principles are increasingly being considered in many areas where reliable data about the shape, the surface properties, the state of stress and the strength of the object under test have to be acquired. However, these advantages have to be paid with some serious disadvantages that are mainly connected with the poor features of identification problems. In this article several examples are presented where optical metrology is helpful for experimental mechanics. The presentation is mainly focused on two topics: the acquisition of quantitative data for experimental stress analysis and the solution of inspection problems by holographic non-destructive testing. Some current aspects such as modern approaches for the solution of identification problems, the installation of remote laboratories and the calibration of measurement set-ups by specially engineered calibration samples are discussed finally.

1. Introduction

Look quickly but don´t touch is an important rule not only for modern measurement and testing systems in industrial quality control but also for many related inspection tasks. What is required are measurement and inspection techniques that are very fast, robust, and relatively low cost compared to the products being investigated. Modern full-field optical methods such as holographic interferometry, speckle metrology, moiré and fringe projection provide a promising alternative to conventional approaches such as the tactile measurement. The main advantages of these optical methods are: non-contact, nondestructive and fieldwise working principle, fast response, high sensitivity and accuracy (typical displacement resolution of a few nanometers and strain values of 100 microstrain), high resolution of data points (e.g. 1000x1000 points for a sub-mm field of view), and the advanced performance of the system, i.e., automatic analysis of the results and fast data processing in order to meet the requirements of the underlying numerical or analytical model. Consequently, optical principles are increasingly being considered in all steps of the evolution of modern products. Relevant applications cover such important fields as testing of lenses and mirrors with respect to optical surface forms, design optimization of components by stress analysis under operational load, on site investigation of industrial products and artwork having complex structures and surfaces with the purpose of material fault detection and, last but not least optical shape measurement as a meanwhile indispensable tool for the reverse engineering of almost any objects.

The basic principle of the methods considered here consists either in a specific structuring of the illumination of the object by incoherent projection of fringe patterns onto the surface under test or by coherent superposition (interference) of light fields representing different states of the object. A common property of most of the methods is that they produce a fringe pattern as output. In these intensity fluctuations the quantities of interest - coordinates, displacements, refractive index and others - are coded in the scale of the fringe period. Using coherent methods this period is determined by the wavelength of the interfering light fields. In the case of incoherent fringe projection the spacing between adjacent lines of the projected intensity distribution can be tuned very flexible by modern spatial light modulators with the purpose to control the sensitivity and scale of the measurement.

In the following chapters several examples are presented where optical metrology is helpful for experimental mechanics. The presentation is mainly focused on two topics: the acquisition of quantitative data for experimental stress analysis and the solution of inspection problems by holographic non-destructive testing. Some current aspects such as modern approaches for the solution of identification problems and the installation of remote laboratories are discussed finally. However, to emphasize the special quality of optical metrology as a procedure where an inverse problem has to be solved we start with a short discussion of the peculiarities of identification problems.

2. Some Words about Identification Problems

The problems in optical metrology are very similar to those of computer vision. Both disciplines process image like input and use methods of image analysis to derive a symbolic description of the image content or to reconstruct various physical quantities from the acquired intensity distribution. The well known paradigm of Marr [1], according to that computer vision is the development of procedures for the solution of the inverse task of the image formation process, describes nothing else as the task to conclude from the effect (e.g. the intensity I(i,j) in the pixel (i,j)) to its cause (e.g. the of the related object point P(x,y,z). In other words, an inverse problem has to be solved. From the point of view of a mathematician the concept of an inverse problem has a certain degree of ambiguity which is well illustrated by a frequently quoted statement of J.B. Keller [2]: „*We call two problems inverses of one another if the formulation of each involves all or part of the solution of the other. Often for historical reasons, one of the two problems has been studied extensively for some time, while the other has never been studied and is not so well understood. In such cases, the former is called direct problem, while the latter is the inverse problem*“. Both problems are related by a kind of duality in the sense that one problem can be derived from the other by exchanging the role of the data and that of the unknown: the data of one problem are the unknowns of the other and vice versa. As a consequence of this duality it may seem arbitrary to decide what is the direct and what is the inverse problem. For physicists and engineers, however, the situation is quite different because the two problems are not on the same level [3]: one of them, and precisely that called the direct problem, is considered to be more fundamental than the other and, for this reason is also better investigated. Consequently, the historical reasons mentioned by Keller are basically physical reasons.

Processes with a well-defined causality such as the process of image formation in optical metrology are called *direct problems*. Direct problems need information about all quantities which influence the unknown effect. Moreover, the internal structure of causality, all initial and boundary conditions and all geometrical details have to be formulated mathematically [4]. To them belong well-known initial and boundary value problems which are usually expressed by ordinary and partial differential equations. Such direct problems have some excellent properties which make them so attractive for physicists and engineers: If reality and mathematical description fit sufficiently well, the direct problem is expected to be uniquely solvable. Furthermore it is in general stable, i.e. small changes of the initial or boundary conditions cause also small effects only.

Unfortunately, numerous problems in physics and engineering deal with unknown but non-observable values. If the causal connections are investigated backwards we come to the concept of *inverse problems*. Based on indirect measurements, i.e. the observation of effects caused by the quantity we are looking for, one can try to identify the missing parameters. Such problems also called as *identification problems* are well known in optical metrology: the recognition and interpretation of subsurface flaws using ONDT and the reconstruction of phase distributions from the observed intensity. Inverse problems have usually some undesirable properties: they are in general ill-posed, ambiguous and unstable. The concept of *well-posedness* is addressed here.

The concept of well-posedness was introduced by Hadamard [5] into the mathematical literature. He defined a Cauchy-problem of partial differential equations as well-posed, if and only if, for all Cauchy-data there is a uniquely determined solution depending continuously on the data; otherwise the problem is ill-posed. In mathematical notation an operator equation

$$F(x) = y \tag{1}$$

is defined as well-posed with a linear operator $F \in \pounds(X,Y)$ in Banach spaces X and Y if the following three Hadamard conditions are satisfied [5]:

1. $F(x)=y$ has a solution $x \in X$ for all $y \in Y$ (existence),
2. This solution x is determined uniquely (uniqueness),
3. The solution x depends continuously on the data y, i.e., the convergence $\|y_n-y\| \to 0$ of a sequence $\{y_n\}=\{F(x_n)\}$ implies the convergence $\|x_n-x\| \to 0$ of corresponding solutions (stability).

If at least one of the above conditions is violated, then the operator equation is called ill-posed. Simply spoken ill-posedness means that we have not enough information to solve the problem uniquely.

In order to overcome the disadvantages of *ill-posedness* in the process of finding an approximate solution to an inverse problem, different techniques of *regularization* are used. Regularizing an inverse problem means that instead of the ill-posed original problem a well-posed related problem has to be formulated. The key decision of regularization is to find out an admissible compromise between stability and approximation [6]. The formulation of a sufficiently stable auxiliary problem means that the original problem has to be changed accordingly radically. As a consequence one cannot expect that the properties of the solution of the auxiliary problem coincide with the properties of the original problem. But convergence between the regularized and the original solution should be guaranteed if the stochastic character of the experimental data is decreasing. In case of noisy data y the identification of unknown quantities can be considered as an estimation problem. Depending on the linearity or non-linearity of the operator F, we than have linear and non-linear regression models, respectively. Consequently, least-square methods play an important role in the solution of inverse problems:

$$\|F(x)-y_\varepsilon\|^2 \to \min \tag{2}$$

with $y_\varepsilon=y+\varepsilon$.

For the solution of inverse/ill-posed problems it is important to apply a maximum amount of a-priori knowledge or predictions about the physical quantities to be determined. Always the question has to be answered if the measured data contain enough information to determine the unknown quantity uniquely. In case of direct problems where the data result from the integration of unknown components data smoothing happens. As an example may serve the response of a fault under the surface to an applied load. The effect can only measured at the surface after the answer of the fault propagates through the material. Consequently, the direct problem is a problem directed towards a loss of information and its solution defines a transition from a physical quantity with a certain information content to another quantity with a smaller information content. This implies that the solution is much smoother than the corresponding object. Consequently, the information about certain properties of the defect gets lost and therefore very different causes may cause almost the same effect after integration. The ambiguous relation between the observed fringe pattern appearing on the surface and its corresponding cause under the surface - the material fault – is a well known example for specialists in HNDT. The response of the fault to the applied load is smoothed since only the displacement on the surface gives rise to the observed fringe pattern. Because of the mentioned integration process these fringe patterns show a limited topology [7,8]. On the other hand, a big variety of different fringe patterns can be observed depending on the structural properties of the object under test, the existing faults and the applied loading. Therefore, the practical experience shows that fixed recognition strategies based on known flaw - fringe pattern relations are successful only if the boundary conditions of the test procedure are limited in an inadmissible way. Since such conditions cannot be guaranteed, generally more flexible recognition strategies – we call them *active strategies* [8,9] - have to be developed. Most of the ”classical” regularisation procedures [4, 10] refer to a spatial neighbourhood and are applied in passive methods of image analysis. In contrast to these passive methods active approaches in optical metrology prefer another way to handle the difficult regularization problem (see §4) [11].

3. Optical Metrology for Experimental Stress Analysis

There are many examples where modern optical metrology has already proven its advantages for the solution of problems in experimental stress analysis such as the reconstruction of material parameters in microsystems technology [12,13]. The increasing trend towards miniaturization has caused a dramatic progress in the development of Micro-Electro-Mechanical Systems (MEMS) and Micro-Opto-Mechanical Systems (MOEMS). However, the reliability of such systems is an important issue that still requires advanced research. For the quality inspection, it is not only necessary to know their geometry but also the displacements or deformations due to mechanical, thermal or electrostatic loads. The measurement of the deformation of micro-mechanical systems may be used for the calculation of strain and the knowledge about the applied forces allows in combination with corresponding material laws the derivation of stresses and material parameters as well. This information may then be used for the validation of FEM models and for the detection of any imperfections in microsystems. Since the structures themselves exhibit typical dimensions of the order of some micrometers, it is necessary to measure the deformation with an accuracy in the nanometer range. A set of non-contacting procedures suitable for the measurement of shape, roughness, deformations and strain of small objects has been developed over the last years [14]. The potential of such methods has been demonstrated, and shape and roughness measurement systems are currently used in industry. Techniques for the measurement of deformation and strain have been successfully tested in the laboratory; so far, their use in an industrial environment takes place however in few cases only. A deficit is that calibration procedures are not available yet or, more precisely, these have only been developed for macroscopic components [15]. Therefore we start with the presentation of a calibration sample that was developed recently for the calibration of measurement setups in microcomponents testing [16], then we show some examples for the determination of shape and displacement data on example of digital holography and finally the reconstruction of material parameters is discussed. Fig. 1 shows a schematic outline of the evaluation process on example of holographic techniques.

3.1 Calibration of the Measurement Setup

The different steps necessary for the calibration of a setup for the measurement of MEMS are schematically shown in Fig. 2 and demonstrated as follows. This procedure has a general character and the designed reference devices may be used for calibrating different measurement systems applied in the laboratory or the production environment. The applied reference devices should have small dimensions (MEMS generally range in size from a micrometer to some millimeters) and surface finish typical of microsystems. The reference can be regarded as MEMS itself, which meets particularly high requirements in terms of reproducibility and stability. Microdevices are built using materials with different mechanical characteristics in order to be able to perform different functions (e.g. actuator, sensor), and their surfaces are usually characterized by low roughness (few nanometers). Silicon (Si) is the mostly used material for the fabrication of MEMS. Consequently, the reference materials use a silicon substrate coated with elements made of polycrystalline silicon and metal electrodes.

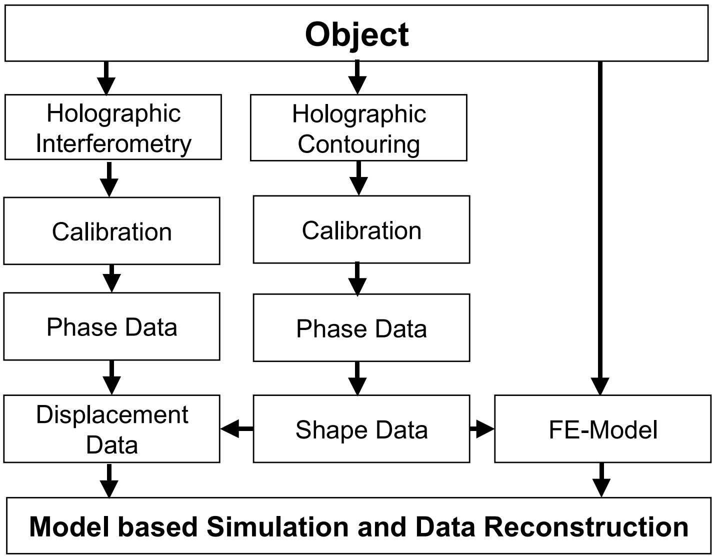

Fig. 1: Evaluation scheme of material properties based on a combined shape and deformation measurement

Several references are needed in order to cover the different translation and deformation principles typically used in MEMS: 1D translation, 2D and 3D translation, Rotation around several axes, 1Dand 2D tensile strain, and 1D … 3D dynamic deformation (vibration). All these modifications must be generated in a reproducible way by application of defined loads. Traceability (which is defined as an unbroken chain of measurements relating an instrument's measurements to a known standard) is a crucial issue; it is thus necessary to have a well-defined chain that relates the deformation of the reference microsystem to the International System of Units (SI). A reliable and common way of obtaining reproducible displacements and deformations in MEMS is to activate them by means of an electric potential difference (Volts, V) which induces a given translation or surface deformation (meters, m). The chain from the voltage application to the deformation can be clearly described by simple physical rules.

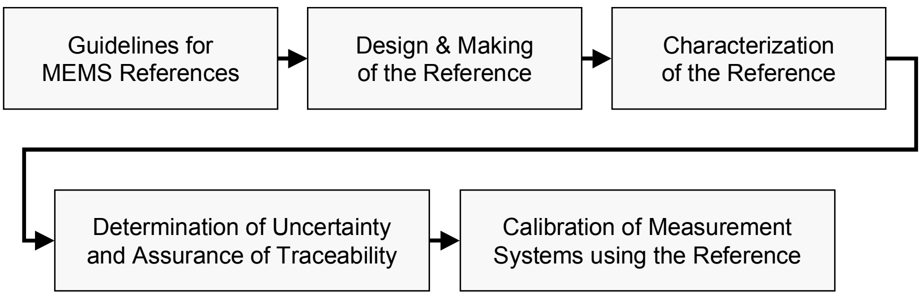

Fig. 2: Strategy for the calibration of optical measurement systems for the inspection of microcomponents by using especially designed MEMS references

Two types of reference devices were designed and fabricated to ensure a calibration of 3D-measurement systems: a 1D in-plane translation sample and an out-off-plane sample (see Fig. 3) [16,17]. The in-plan device, for instance, consists of an inner movable part connected to an outer fixed frame through 1125-µm-long, 10-µm-wide springs, obtained from the active layer of silicon-on-insulator (SOI) by a common technology employing deep reactive ion etching (DRIE) of crystalline silicon followed by an HF-based release step, which selectively removes the oxide (insulator) layer at the end of the process, leaving the movable parts suspended. The total size of the structure is 7x7 mm² but the moving parts inside are much smaller. A particularity of such layout is that uni-axial, in-plane displacements are insured by geometrical constraints. The motion of the central part of the microactuator can be obtained from both mechanical and electrostatic mechanisms, by applying a voltage to a comb-drive exciter (500 fingers each 10-µm-wide, spaced by 4 µm) or by inserting the tip of an external actuator in a predefined window opening on the chip. The calibration procedure is described in [16,17,18].

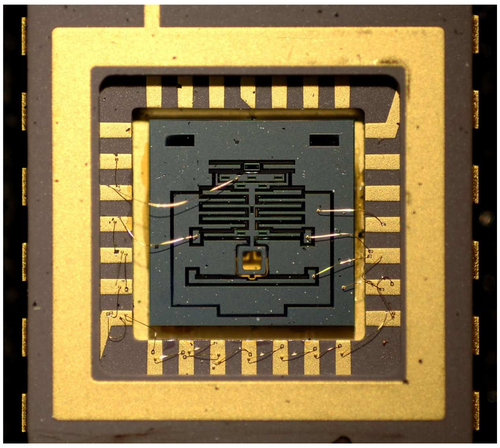

Fig. 3a: In-plane calibration sample

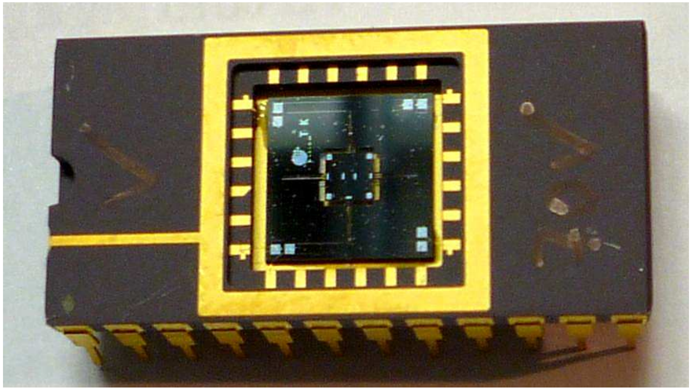

Fig. 3b: Out-off-plane calibration sample

3.2 Shape and Displacement Measurement of Small Components by Digital Holography

To demonstrate the combined shape and displacement measurement by digital holography as test object a small electrical 2.2kΩ resistor is used, Fig. 4a. Its shape is registered using the multi-wavelengths technique [19]. The differences of the wavelengths are $\Delta\lambda$ = 0.03nm, 0.5nm and 3.0nm (at a working wavelength of λ = 591,01nm). This results in synthetic wavelengths of 1.16cm, 0.7mm and 117µm, Fig. 4b,c,d. Here one fringe represents approximately half of the synthetic wavelength. The hierarchical unwrapping algorithm [19] was applied and finally the phase map was transformed into a height map (Fig. 4e). The result is plotted as a 3d-plot for a better visualization, Fig. 4f. For the inspection of the thermal behavior of the resistor an electrical voltage is applied that causes a heating and deformation of the surface. Due to the applied voltage the resistor was heated from 28,84°C to 37,44°C. The wrapped and unwrapped interferograms, Fig 5a, b, show the phase difference of the digitally reconstructed phases before and after the thermal loading. The fringes in Fig. 5a represent the deformation in the direction of one of the sensitivity vectors. Each fringe represents a deformation of about $\lambda/2$ or 295nm. The 3d-plot in Fig. 5c shows the displacement field as small arrows on the surface of the object. The deformation is magnified by a factor 106 relatively to the shape. The measured data were compared with measurements performed by a scanning triangulation sensor of high precision (≈100nm). Matching the shape data sets shows that the noise level of the interferometric method is about 1:20 of the smallest synthetic wavelength λ_{syn}^{n}. In this example the uncertainty in the measurement data is ±6µm.

3.3 The determination of material parameters of microcomponents using digital holography

The implemented system described in the following is a first step in the direction of a reliable determination of material parameters with optical metrology [13,14]. It is based on a consistent interferometrical shape and deformation analysis in combination with adapted loading equipment. The precise measurement of coordinates, displacements and forces allows the determination of several material parameters like the Poisson-ratio, the Young's modulus and the thermal expansion coefficient. For the evaluation of the system performance an appropriate class of test samples was created consisting of micro silicon beams, membranes and tongues [20].

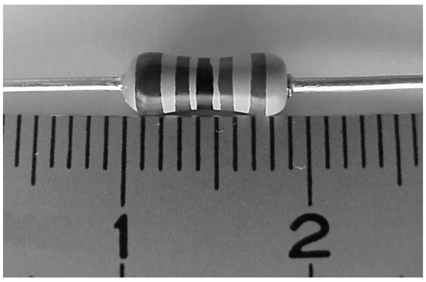

a) Photograph of the resistor (ruler scale is cm)

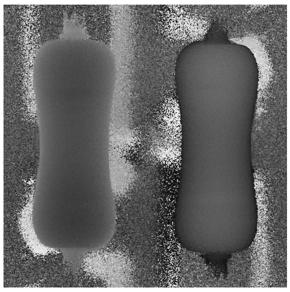

b) Wavelength Contouring Interferogram with Δλ = 0.03nm

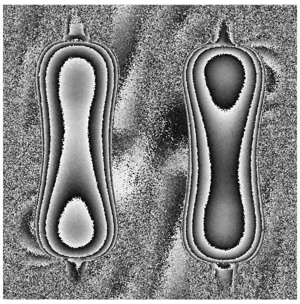

c) Wavelength Contouring Interferogram with Δλ = 0.5nm

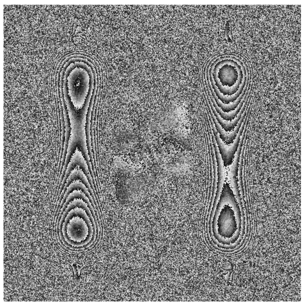

d) Wavelength Contouring Interferogram with Δλ = 3.0nm

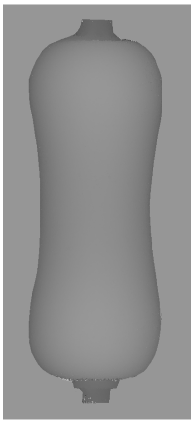

e) Unwrapped interference phase

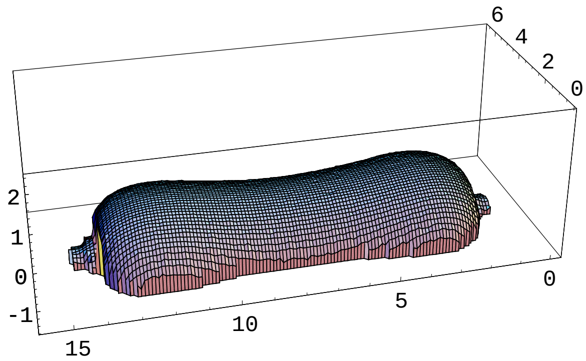

f) 3d plot of the shape of the resistor

Fig. 4: Shape measurement of a resistor using digital holography and multi-wavelengths contouring

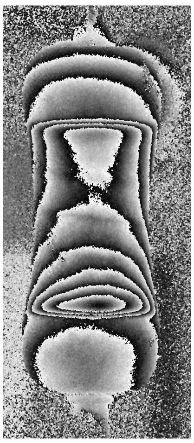

a) mod 2π interference phase

b) Unwrapped interference phase

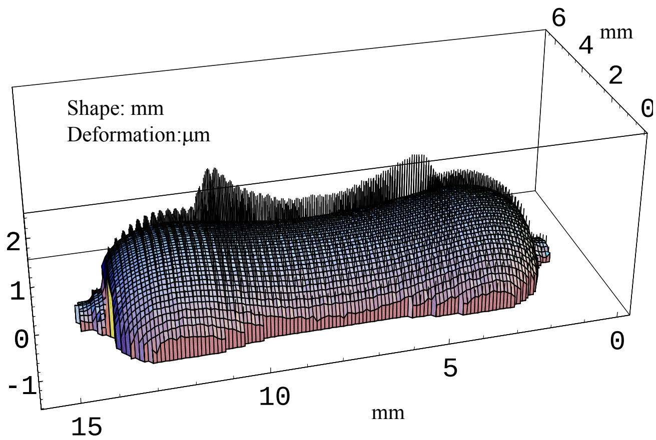

c) Combined shape and deformation plot of the resistor..

Fig. 5: Displacement field of the heated resistor

The schematic set-up of the optical part is shown in Fig. 6a. The compact digital-holographic interferometer consists of an optimized arrangement with 4 illumination directions and 1 observation direction to measure the 3D-displacements and coordinates precisely, Fig. 6b.

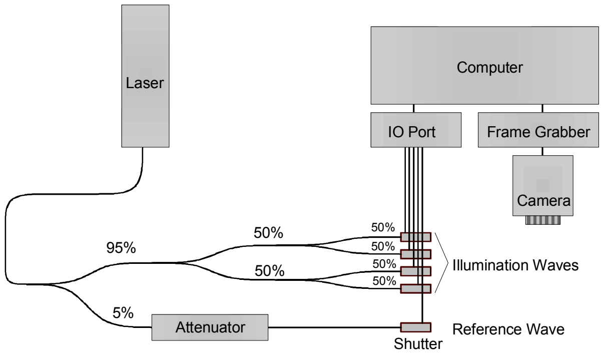

a) Schematic set-up of the interferometer

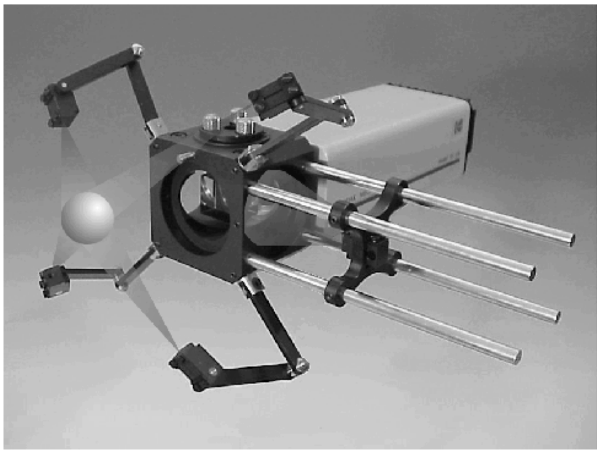

b) Compact digital holographic interferometer with 4 illumination directions

Fig. 6: The compact digital-holographic interferometer [13]

a) The determination of the Poisson ratio of microbeams

The physical models used for the determination of the material's properties can be of any desired complexity. Simple models are easy to handle but imply errors in the evaluation of the physical quantities. Thus material properties should always be specified together with the applied model. For the demonstration of the whole measurement procedure we prefer rather simple models that assume linear elastic behavior of the specimen. The determination of the Poisson ratio by holographic interferometry is a well known example of the efficiency of coherent-optical methods [21]. Digital Holography provides a relatively simple way to determine this quantity. Moments of force are applied to a rectangular sample at opposite sides. Fig. 7a shows a typical loading machine designed especially for small objects. The small dimensions of the samples demand a precise adjustment of all components. Unwanted torsions of small magnitude are corrected numerically which is easy with the use of the mod 2π-phase maps from digital holography [22]. The deflection causes hyperbolic fringe structures, Fig. 7b. Conventionally, the Poisson ratio is derived numerically from the angle between the asymptotic lines of the fringes of equal phase [21]. The deformation can be formulated in first order approximation by the following equation.

$$u(y,z) = -\frac{1}{2R}\left[y^2 + \upsilon\left(a^2 - z^2\right)\right] \tag{3}$$

Here u means the deformation in x-direction at position (y,z) on the surface of the object. ν stands for the Poisson ratio. R is the radius of curvature and a is a parameter which will not be of any importance during the following evaluation process. R results from a slight deflection in the initial state. This helps to ensure a proper mechanical contact between the support and the sample. Eq. (3) makes clear that the upper and lower surface of the sample are deformed to parabolic curves where the inside is bent in a convex way and the outside is curved in a concave way. Since this analytical model contains the Poisson ratio as a parameter it is possible to use the measured deformation for its evaluation. This is performed numerically by approximating the model to the data (Fig. 7c) with a least-square-fit, Fig. 7d.

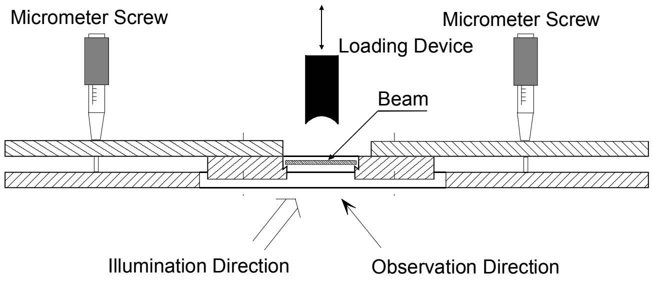

a) Schematic experimental setup

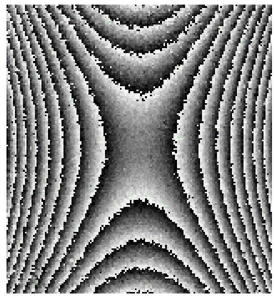

b) Reconstructed mod 2π-phase map

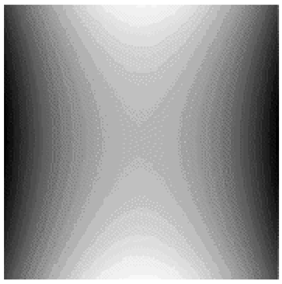

c) Unwrapped phase field

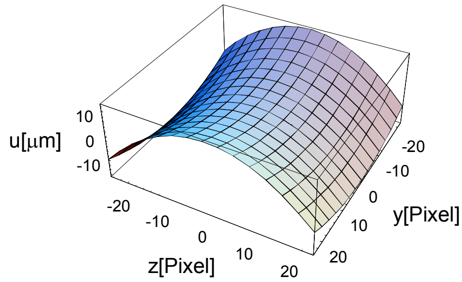

d) Approximated function according Equ. (3)

Fig. 7: The measurement of the Poisson ratio by Digital Holography

The values obtained by this method show a good reproducibility and accuracy in comparison to conventional optical techniques for small samples. Table 1 contains some of the results for beams made of spring steel, structural steel and titanium. The values correlate with the values given by the manufacturers within the tolerances of the material batches [13].

Material	Width [mm]	Thickness [mm]	Length [mm]	Poisson ratio: measured & [literature]
spring steel	1,2	0,2	12	0,288 [0,29-0,31]
spring steel	2,0	0,1	12	0,301 [0,29-0,31]
structural steel	1,0	0,5	10	0,338 [0,29-0,31]
structural steel	1,5	0,5	10	0,345 [0,29-0,31]
titanium	2,0	0,8	10	0,359 [0,361]
Titan	1,5	0,8	10	0,381 [0,361]

Table 1: Measured Poisson ratio of different materials

b) The determination of the Young's modulus of microbeams

The Young's modulus can be determined in a similar way as the Poisson ratio if the physical model contains this quantity as a parameter. We use small silicon beams as shown in Fig. 8 which are clamped at one edge and mechanically loaded with a defined force at the opposite edge. The 3d-surface displacements **d**(u,v,w) (Fig. 8c) can be measured with the interferometer by evaluating at least 3 interferograms (Fig. 8b) mde with different illumination directions [23]. A model of the beam bending containing the Young's modulus E as a free parameter is the basis for a numerical fit of the experimental values:

$$u(y) = \frac{Fl^3}{6EI_y}\left(2 - 3\frac{y}{l} + \frac{y^3}{l^3}\right) \tag{4}$$

u is the displacement in x-direction, y a position on the beam of the length l. I_y is the axial moment of inertia in the (x,z)-plane that can be estimated with the help of a shape measurement. F is the force applied to the tip of the beam. The applied forces are relatively small so that a special loading mechanism was developed, Fig. 8a. The spring constant k is assumed to be known precisely as well as the displacement $\Delta a = a - a'$. With this information the force can be evaluated with the equation

$$F = k\,\Delta a \tag{5}$$

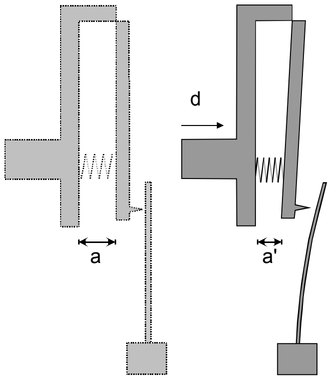

a) Working principle of the loading mechanism for the small samples

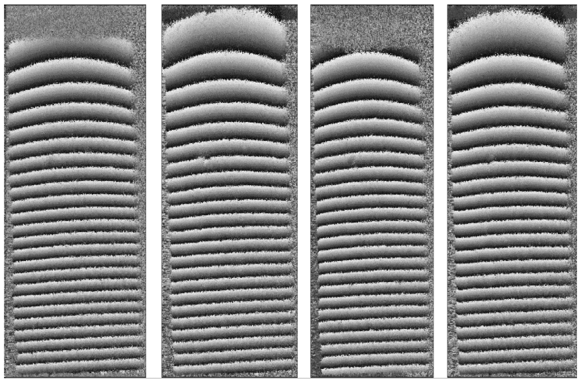

b) 4 interferograms recorded from four different illumination directions

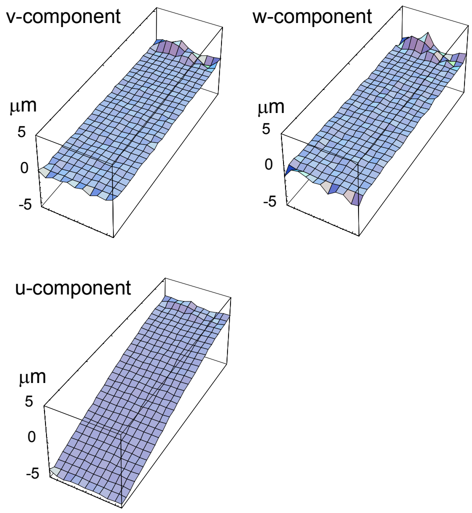

c) Deformation calculated in Cartesian coordinates (scale of the plots in µm)

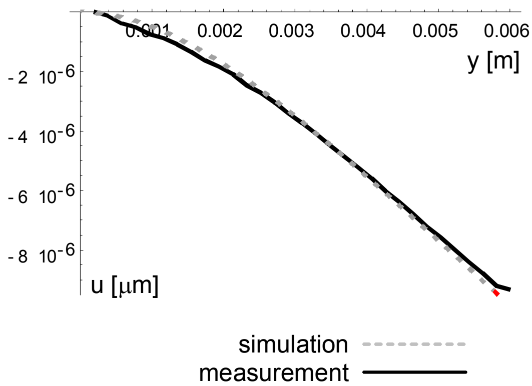

d) Profile of the deformation in x-direction

Fig 8: Determination of Young's modulus by digital holography

Several experiments with thin beams made of silicon (dimensions: length 3mm, width 1mm) delivered an average value of E=162MPa. The literature value (in the considered crystal direction) is about 166MPa. These values can vary in a big range according to the material's history, treatment and degree of impurity.

c) The determination of the thermal expansion coefficient of microbeams

For the interferometric investigation of the thermal behavior of various specimens it must be ensured that thermal turbulences and non-uniform temperature distributions are avoided. Therefore a vacuum chamber that can be supplied with adapted loading devices was constructed, Fig. 9a. The used thermal loading device is capable of keeping a constant temperature within an accuracy of 0,02°C in a range of about 20°C up to 180°C. The holographic interferometer was mounted outside at the observation window of the chamber, Fig. 9b.

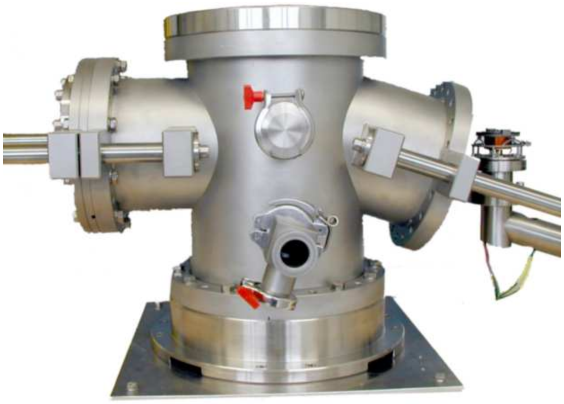

a) Vacuum chamber with the supply channel

b) Interferometer mounted on the inspection window

Fig. 9: Inspection system for the investigation of micro-components with respect to material parameters (the device shown in Fig. 9a is made by CWM Chemnitz)

As a test object a mono-crystal silicon beam with 4,5 Ωcm phosphor coating was used. The interferograms are recorded at different temperature differences. The complete evaluation process can be summarized as follows:

- the geometry of the setup was measured to get the geometry matrix for the evaluation of the 3 displacement components,
- 4 holograms are recorded in the initial state of the object,
- the object is loaded thermally and recorded holographically from four different illumination directions,
- the displacement vector components (u,v,w) are calculated based on the evaluation of the 4 interferograms,
- rigid body motions are separated from internal deformations of the object itself by subtracting the mean movement from the displacement values.

The absolute length change ΔL is determined as well as the total length of the beam which can be performed by using the imaging properties of Digital Holography. The thermal expansion coefficient in y- and z-direction can simply be calculated by using the equation

$$\alpha = \frac{\Delta L}{L_O \Delta T} \tag{6}$$

The extension in x-direction is too small to be detectable with the applied method.

As an example the thermal expansion coefficient α of a small 2mm x 9mm x 100µm mono-crystal silicon beam is measured. Fig. 10 shows the four resulting interferograms. The applied temperature difference ΔT was 30°C. After elimination of the rigid body motion the three deformation components are evaluated as shown in Fig. 11. Considering the dimensions of the beam we receive a value for α of about $\alpha = 2{,}92\times10^{-6}$ 1/K. The literature values vary in a big range due to different measurement methods, conditions and material batches: $\alpha = 2{,}4 \,..\, 6{,}7\times10^{-6}$ 1/K.

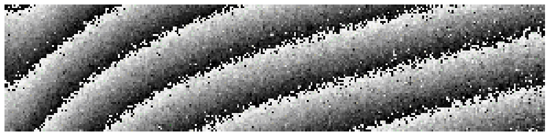

a) Illumination direction 1

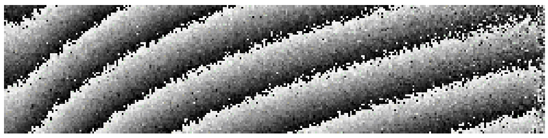

b) Illumination direction 2

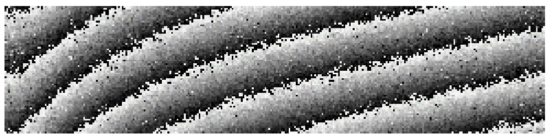

c) Illumination direction 3

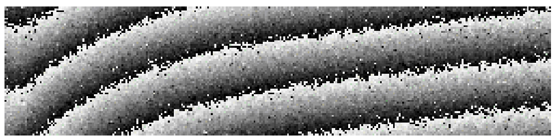

d) Illumination direction 4

Fig. 10: 4 interferograms due the deformation of the object by thermal load

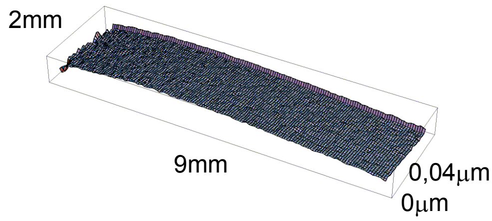

a) u-component

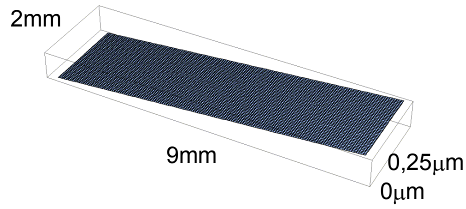

b) v- component

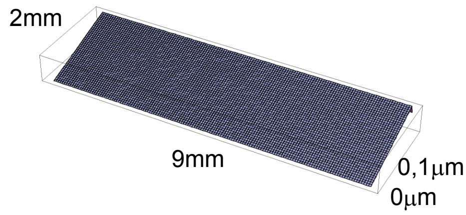

c) w-component

Fig 11: 3d-displacement components (u,v,w)

4. Optical Metrology for Non-Destructive Testing

Modern optical measurement techniques such as fringe projection, moiré techniques, holographic and speckle metrology can be applied not only for high precision quantitative analysis of displacement and strain fields (see §3) but also for *non-destructive inspection* of simple objects and complex structures with regard to surface and internal *flaws*. These flaws are recognized by the evaluation of the resulting fringe patterns with respect to characteristic pattern irregularities as for instance "bull eye"-fringes, distorted fringes, locally compressed fringes, dissected and mutually displaced fringes. Based on practical experience and knowledge about the material behaviour as well as on the boundary conditions of the experiment the flaw can be classified as e.g. *void*, *debond*, *delamination*, *weak area*, *crack* or similar imperfection. The methods have been applied successfully for industrially relevant testing problems in different fields: quality control of circuit boards and electronic modules, inspection of satellite fuel tanks and pressure vessels, tire testing, glass and carbon fibre reinforced material testing, investigation of turbine blades, automobile engine and car body inspection, building and artwork inspection, see e.g. [24]. However, the automatic evaluation works not perfect in many cases, since the recognition and classification of fault indicating patterns in a fringe patterns is often more difficult than the quantitative phase reconstruction in displacement and shape measurement. The task consists not only in the automatic recognition of complex patterns within noisy images but also in the systematic evaluation of these patterns with respect to their cause. First results were reported by Glünder et al. [25] in 1982. In this work an opto-electronic hybrid processor was used for fast and effective data reduction. A complete digital system for the analysis of misbrazing in brazed cooling panels was proposed by Robinson [26] in 1983. When the plate is slowly pressurized misbrazing is observed as a closed-ring fringe pattern before the standard deformation pattern appears. However, the published evaluation procedure was very time consuming. Another approach [27] that applies parallel hardware was proposed in 1987. In less than one minute the skeleton of the fringe pattern was derived and two line features (density and curvature) were determined to recognize flaw induced patterns. Statistical methods have been applied to the fringe system, since the beginning of automatic evaluation, in order to detect inhomogeneities [28]. The idea was to detect anomalously higher and lower fringe densities in either the spatial or frequency domain. This works quite well for simple geometries. However, when the geometry of the component is complex, the fringe system becomes complex and will often contain inhomogeneities even in the absence of defects. So these methods fail for widespread application of HNDT. The fact, that skilled operators can detect fault-indicating fringe pattern changes even in complex structures leads to the approach of using processing techniques which apply knowledge to the evaluation of the fringes.

The basic idea in *optical non-destructive testing* is that a component with a fault will react in a different manner compared to a sound structure, since the stiffness or the heat conductivity will be modified locally or globally. The response of the object on a suitable load results in characteristic fringe patterns when optical methods such as holographic interferometry, shearography or other are applied, Fig. 12a. The fringe pattern - an example is given in Fig. 12b - can be evaluated to determine the displacement and the deformation. However, in ONDT the objective is not to evaluate surface deformations quantitatively but to determine unacceptable local deformations identified by inhomogeneities in the fringe pattern. The task consists in the detection of fault-indicating fringe irregularities and in its classification with respect to the fault that caused them. However, not all inhomogeneities indicate a defect. Consequently, experience and a-priori knowledge about the object and its respons to artificial and working loads, respectively, is very important for ONDT

The most obvious deficit in all published procedures is the insufficient capability for *flaw classification*. Two modern approaches have good potential to overcome this unsatisfactory situation. The first one applies *knowledge-based systems* or *neural networks* to "learn" different kinds of flaws from simulated or practical examples [29,30]. The second approach combines model-based simulation methods and practical measurements [11,31,32]. Here the iterative and model-based approach is described shortly [31].

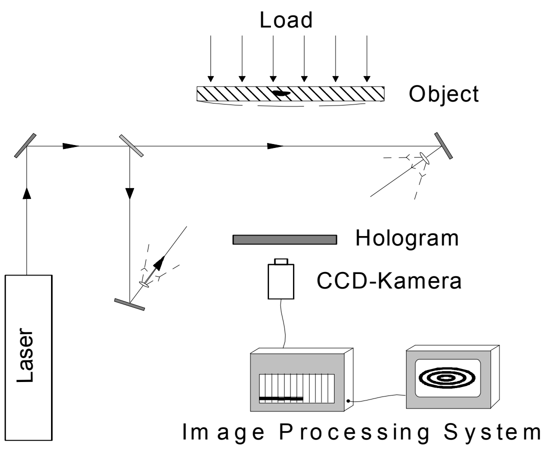

a) Set-up for holographic non-destructive testing interferometry

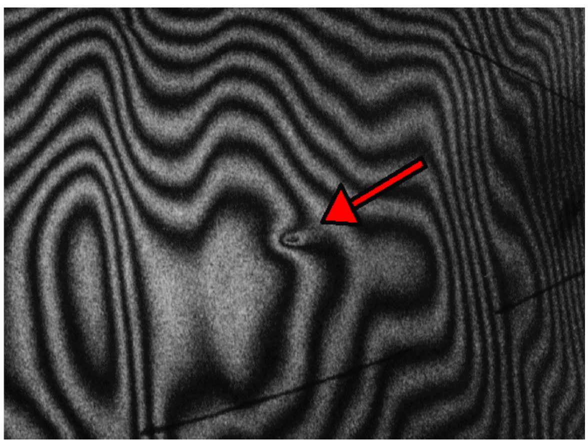

b) Example of an interferogram with a flaw (subsurface void) indicating pattern

Fig. 12: Optical non-destructive testing by holographic interferometry (HNDT)

Following the current trend in image analysis more flexibility in the processing strategy is obtained by combining the classical data driven *bottom-up strategy*, Fig. 13a, with the so-called expectation driven *top-down strategy* [33], Fig. 13b. The first strategy has been proven to be very efficient but extra effort must be paid to obtain a high image quality and in most cases a-priori knowledge has to be added by operator interaction to derive an unambiguous solution. The image formation process is considered as a rather fixed/passive data source and is not actively involved in the evaluation process.

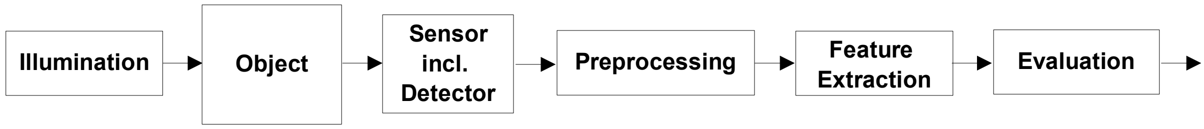

a) Passive approach: classical data driven bottom-up strategy

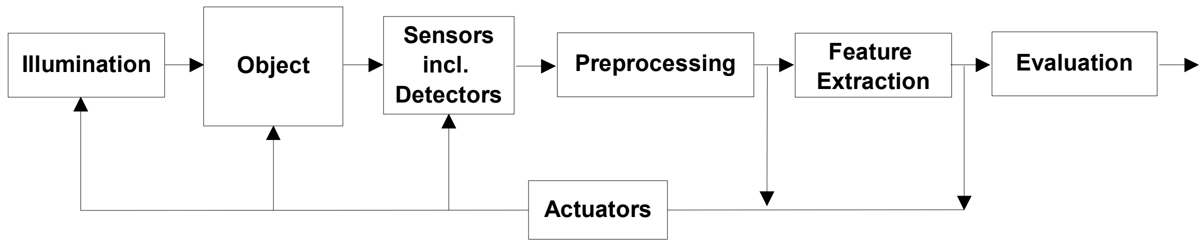

b) Active approach: combination with the expectation driven top-down strategy by driving a feedback loop between the components responsible for image analysis and image acquisition

Fig. 13: Different image processing strategies

In contrast to this approach the second strategy includes the image formation as an active component in the evaluation process. Dependent on the complexity of the problem and the state of evaluation new data sets are actively produced by driving a feedback loop between the system components which are responsible for data generation (light sources, sensors and actuators) and those which are responsible for data processing and analysis (computers). Support from other sensors at different positions, recordings from different time instances or the exploitation of different physical sensor principles, i.e multi-sensor approaches, are considered in that concept [8,9]. The strategy which supervises the image analysis is connected to and controlled by the information gathered by sensors and by a knowledge base. This data base contains the relevant knowledge about the application, the scene which has been imaged and the image acquisition/processing methods.

The active approach discussed here combines the knowledge about the pattern formation process with the possibilities of modern CAE-tools [31, 34]. The basic idea of the model-based approach and the implemented processing chain are shown in Fig. 14. At the beginning an interferometric measurement (e.g. made with holographic interferometry, EPSI or shearography) creates an interferogram containing information about the object under test. Fig. 15a. shows the holographic interferogram of a model of a satellite tank made from aluminium and loaded with inner pressure [35]. A first analysis (e.g by skeletonization or phase shifting) and feature-extraction allows to make a hypothesis about the object and its fault. This hypothesis serves as a basis for a finite-element model of the object including the fault and considering the experimental conditions, Fig. 15c and 15d. With the known circumstances of the experimental set-up a synthetic interferogram of the object is generated, Fig. 15b, followed by a second analysis and feature-extraction. All properties (patterns, phase values and relevant features) of both interferograms are compared to decide if the supposed hypothesis is correct [36]. If the difference between the calculated and the measured pattern is too big, an iterative process is started to improve the conformance. In that process the hypothesis is modified in combination with a manipulation of the load (strength and/or type) or other known boundary conditions. The active approach considers also the generation of a sequence of interferograms caused by a continuous increasing/decreasing of the load and/or a change of the kind of load (thermal load, pressure load, ...). As the result of this iterative approach an improved hypothesis containing the desired information such as the type of the fault, its criticality, dimension and location is derived. The feedback loop is finished if the comparison between the fringe patterns delivered by the simulation loop (direct problem) and the measurement loop (indirect problem) are in sufficient agreement. The searched fault parameters are defined by the input data of the finite element model of the final interferogram synthesis.

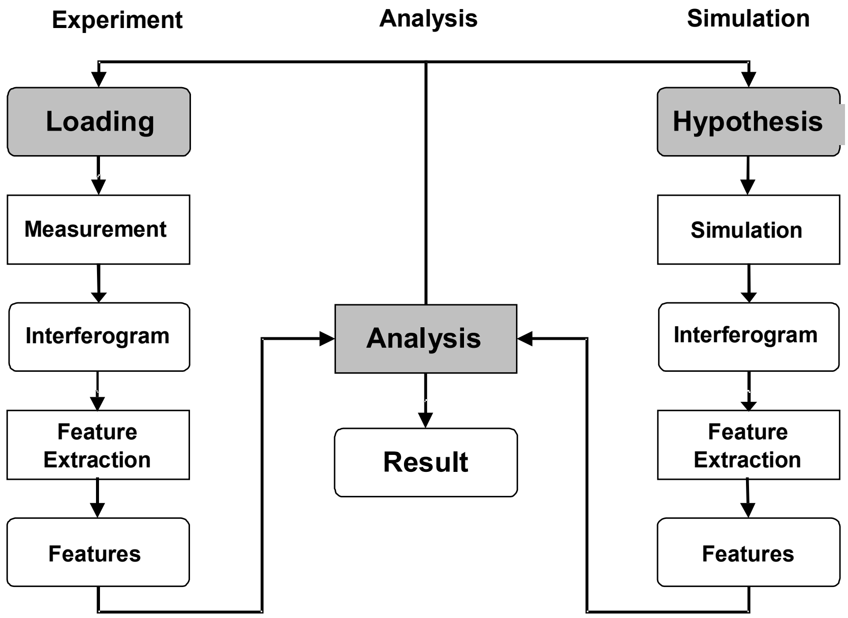

Fig. 14: Implementation of the algorithm “Recognition by Synthesis” in HNDT: feedback loop and combination of a simulation loop for running the direct problem and a measurement loop for running the indirect problem

The fault detected in the given example was a weakening of the inner part of the satellite tank wall with the parameters: spheric shape, depth 0,8 mm, diameter 5 mm. The detection certainty could be improved considerably by an active loading strategy.

5. Remote Metrology and Remote Laboratories for Experimental Mechanics

The idea of remote and virtual metrology has been reported already in 2000 [37,38] with a conceptual illustration by use of comparative digital holography [39], aimed at the comparison of two nominally identical but physically different objects, e.g., master and sample, in industrial inspection processes. In a first step, a digital hologram of the master is generated and stored, allowing transmission through the Internet. This provides instant, global access to the complete optical information of the master object [40]. For comparison, the master hologram is optically reconstructed using a spatial light and projected onto a sample under inspection, resulting in interferometric patterns that can be analyzed to retrieve the difference between the master and the test object. However, the concept of remote and virtual metrology can be extended far beyond this. For example, it does not only allow for the transmission of static holograms over the Internet, but also provides an opportunity to communicate with and eventually control the physical set-up of a remote metrology system. Furthermore, the metrology system can be modeled in the environment of a 3D virtual reality using CAD or similar technology, providing a more intuitive interface to the physical setup within the virtual world. An engineer or scientist who would like to access the remote real world system can log on to the virtual system, moving and manipulating the setup through an avatar and take the desired measurements. The real metrology system responds to the interaction between the avatar and the 3D virtual representation, providing a more intuitive interface to the physical setup within the virtual world. The measurement data is stored and interpreted automatically for appropriate display within the virtual world, providing the necessary feedback to the experimenter. Such a system open up many novel opportunities in industrial inspection such as virtual remote testing and controlling.

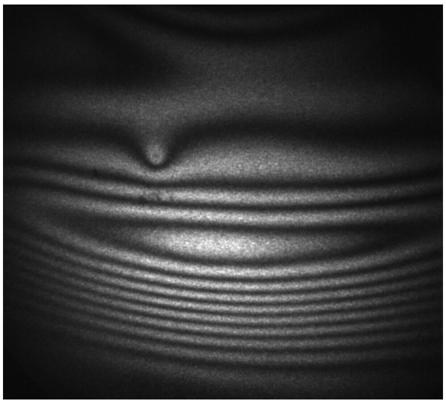

a) Real interferogram of the loaded tank with fault indicating pattern

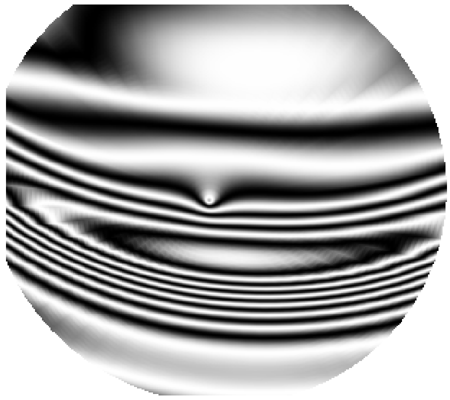

b) Simulated interferogram of the loaded tank with fault indicating pattern

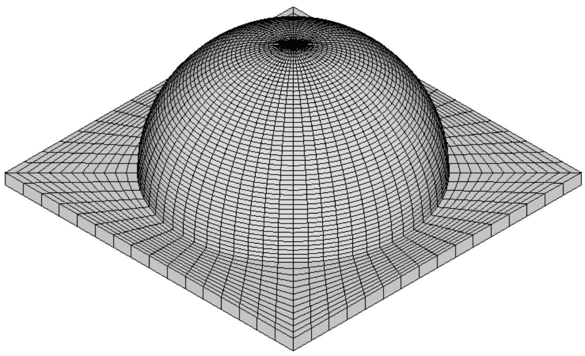

c) FE-model of the satellite tank

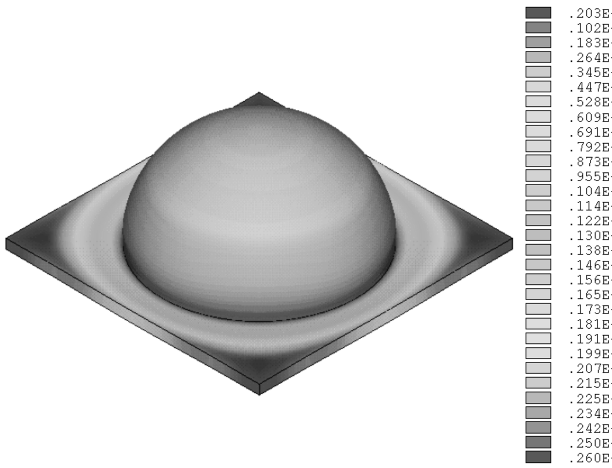

d) Calculated displacement field of the tank loaded with inner pressure

Fig. 15: Recognition by synthesis: Some processing steps on example of a model of a satellite tank with local wall weakening

With the development of broadband Internet and software for remote control, we are able to make progress toward this goal: to build a remote metrology system based on digital holography. Our prototype, being developed within the framework of the BW-eLabs project [41,42], does not intend to implement all the functionality stated above in the current project phase. Instead, we are building a remote experimental system that can perform deformation measurement on small objects such as MEMS under various loads on nanometer scale, and 3D holographic microscopic imaging of (biological) samples on micron scale by providing accessibility from all over the world through Internet connection. The physical hardware is controlled through LabView (National Instruments) and will be connected to a 3D virtual reality, based on the Open Source project Wonderland (Sun). Data storage and retrieval, including a search engine and meta data generation are handled through the Open Source project eSciDoc [43]. The system is primarily designed for deployment in the field of scientific research, in particular for international collaboration in joint experiments. Nevertheless, it is equally useful in education. In the field of chemistry and chemical engineering, such weblabs have been widely employed for education of various curriculum at many international leading universities including MIT in USA and University of Cambridge in the UK [44].

The system architecture for the remote lab is schematically shown in Fig. 16. At the heart of the architecture is the digital holographic microscopic system, which is hidden behind a proxy server and can be accessed directly only by an operator at our institute. The computer running the software necessary for controlling the physical experiment is invisible from the outside. All outside contact is handled by the proxy server, using an SSH tunnel for encrypted, secure data exchange. Users access the experiment through the BW-eLabs portal, which authenticates against an eSciDoc user data base. On successful authentication, an SSH tunnel is opened to the SSH server running on the proxy, with authentication passed on using PAM (``pluggable authentication modules"). eSciDoc also provides storage and access to experimental data, passing data for automatic configuration of the experiment, and access to the publication infrastructure of OPUS (OPUS). From the user's perspective, the functionality of eSciDoc is mostly transparent, working automatically in the background. eSciDoc is accessible by generic users, providing search functionality based on metadata generated during the experiment. The roles and rights of users in eSciDoc are rather complex and can be set individually for each experimental set-up and each set of data (if desired), protecting against undesired third party access while enabling collaboration between privileged partners.

Here we describe the functionality implementation of the architecture, focusing mainly on the setup of the holographic system and the configuration of the remote controlling (i.e. the components in the green box Fig. 16. The experimental setup of the digital holographic microscopic system is shown in Fig. 17. A laser of wavelength λ is first coupled into a fiber, which guides the beam into a fiber coupler that subsequently divides the input laser beam into a reference arm and object arm. The object arm fiber can be switched for different illumination modes, i.e., transmission mode or reflection mode, depending on the property of the object to be investigated. The object is imaged through a 20x/0.5 microscopic objective. The reference fiber is coupled into the system using a beam splitter as shown in Fig. 17 to interfere the reference beam with the object wave. The microscopic table is mounted on an electric-driven 3D positioner (Physical Instrument), allowing the user to shift the field of view at sub-micron precision. A CCD camera (SVS16000 from SVS-Vistek) is placed at a distance x above the microscopic table to record the hologram. The SVS16000 camera has a large sensing area of 43.3 mm diagonally with 16 M (4896x3280) pixels of 7.4x7.4 microns in size, so that a high numerical aperture (NA) can be obtained when it is placed close to the object, even in a lenseless configuration. The hologram $f(\xi,\eta)$ is captured by the camera and is transferred to the computer for subsequent processing. The SVS16000 is a Gigabit Ethernet (GigE) camera, allowing a transmitting rate of as high as 1 gigabit per second, with effect frame rates of *3fps*. It is connected to the host computer through a PCI(e) network interface card with 82541 chip set (for example, Intel Pro/1000 GT PCI card in our case) using an RJ45 network cable.

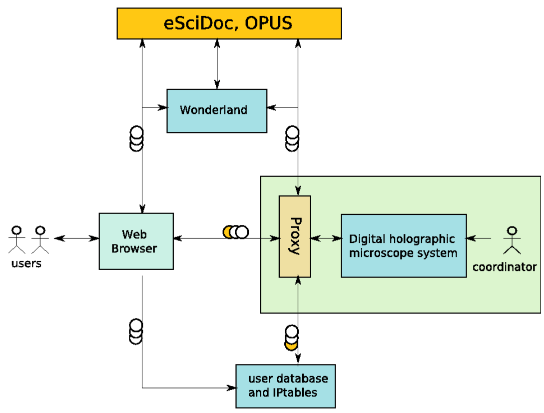

Fig. 16: Schematic architecture for the remote experimental system

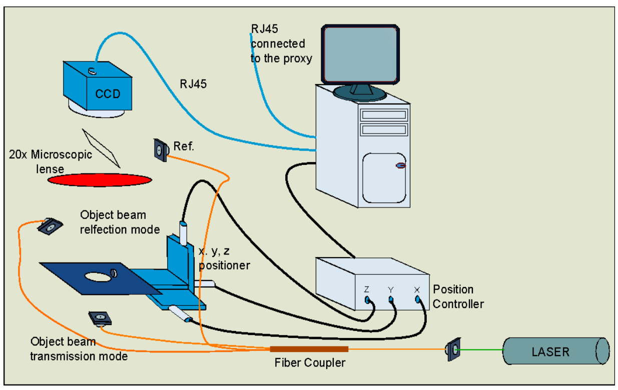

Fig. 17: Experimental setup of the digital holographic microscopic system

Reconstruction of the object wave is performed numerically. The intensity pattern $f(\xi,\mu)$ recorded at the coordinate (ξ,λ) in the CCD-plane is first filtered in the spatial Fourier-domain removing the DC component and the conjugate twin image in the reconstruction. The filtered signal is inverse Fourier transformed and then propagated and focused in the object plane (x,y) at distance z using the Fresnel transformation T(z) (approximation of the wave propagation for distances z >> λ)

$$
\begin{aligned}
g(x,y,z) &= \frac{\exp(ikz)}{i\lambda z}\int_{-\infty}^{\infty} f(\xi,\eta)\exp[\frac{ik}{2z}(x-\xi)^2+(y-\eta)^2]d\xi d\eta \\
&= T(z)(f(\xi,\eta))
\end{aligned}
\tag{7}
$$

The whole reconstruction process can thus be expressed as

$$g(x,y,z) = T(z)\left[F^{-1}(h(F(\xi,\eta)))\right] \tag{8}$$

where F denotes the Fourier-Transform and h the spatial filtering in the Fourier-Domain. Since the project is still ongoing, we provide a demo LabVIEW VI ("Virtual Instrument", the LabView term for a program) to demonstrate the concept. Fig. 17 shows the frontpanel of the LabView VI with the image of a webcam showing the physical setup on the top left, the hologram as recorded by the CCD camera next to it, followed by the numerical reconstruction of the object (in this case, a biological sample, onion cells) to the left. The hologram was filtered in the spatial Fourier-Domain previous to reconstruction, removing the DC component and the twin image in the reconstruction to improve the utilization of the spatial bandwidth of the camera. The other two displays below show the phase retrieved from the hologram and the phase difference between the currently investigated hologram and a reloaded, previously recorded hologram for comparative metrology.

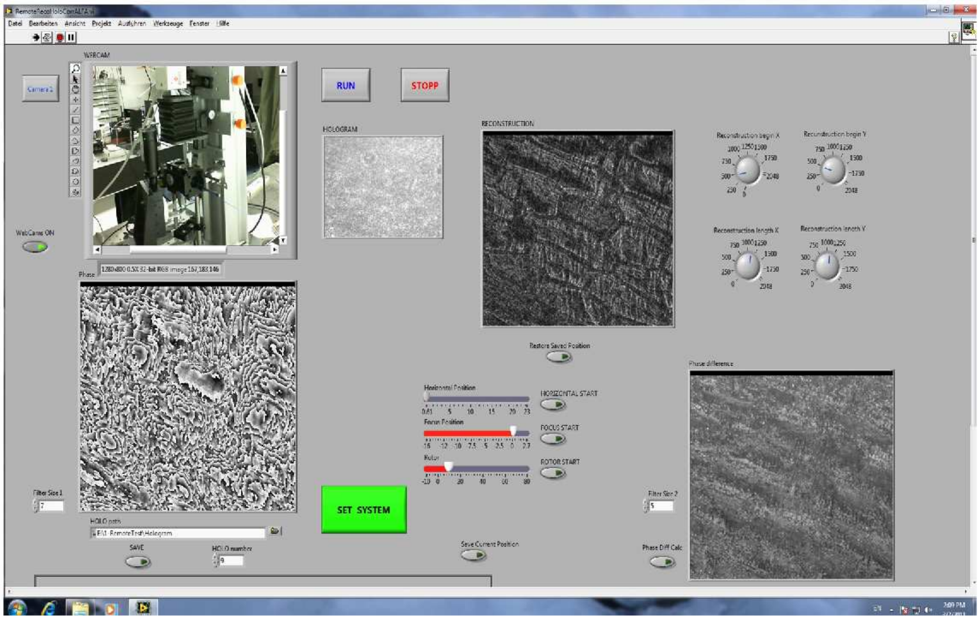

Fig. 17: The current Labview front panel, showing a sample of onion cells

Summary

In this contribution several examples were presented where optical metrology is helpful in experimental mechanics. The presentation was mainly focused on two topics: the acquisition of quantitative data for experimental stress analysis and the solution of identification problems in holographic non-destructive testing. Here an active and model-based strategy was proposed. Some current aspects such as the calibration of measurement setups and the installation of remote laboratories were also discussed.

Acknowledgement
The support by the state of Baden-Württemberg for the project BW-eLabs is kindly acknowledged.

References
[1] Marr, D., "Vision: A Computational Investigation into the Human Representation and Processing of Visual Information. Freeman and Company," San Francisco, 1982
[2] Keller, J.B.,“ Inverse Problems. American Mathematics Monthly," Vol. 83, pp. 107-118, 1976
[3] Bertero, M., and Boccacci, P., Introduction to Inverse Problems in Imaging. Bristol, IOP Publishing, 1998
[4] Tikhonov, A.N., „Solution of Incorrectly Formulated Problems and the Regularization Method,“ Sov. Math. Dokl., Vol. 4, pp. 1035-1038, 1963
[5] Hadamard, J., Lectures on Cauchy‘s problem in partial differential equations. Yale University Press, New Haven 1923
[6] Hofmann, B., „Ill-posedness and regularization of inverse problems – a review of mathematical methods,“ In: H. Lübbig, The inverse problem. Akademie Verlag Berlin 1995, pp. 45-66
[7] Mieth, U.; W. Osten, W. Jüptner: Investigations on the appearance of material faults in holographic interferograms. Proc. Fringe 2001, Elsevier Sc. 2001, pp. 163-172
[8] Osten, W.; Kujawinska, M.: Active phase measuring metrology. In: P.K. Rastogi and D. Inaudi (Eds.): Trends in Optical Nondestructive Testing and Inspection, Elsevier Science B.V. 2000, pp. 45-69
[9] Osten, W.: Active optical metrology - a definition by examples. Proc. SPIE Vol. 3478(1998), pp. 11-25
[10] Tikhonov, A.N., and Arsenin, V.Y., *Solution of Ill-posed Problems*, (Transl. From Russian) Winston and Sons, Washington, 1977
[11] Osten, W.; Elandaloussi, F.; Mieth, U., "Trends for the solution of identifikation problems in holographic non-destructive testing (HNDT)," SPIE Vol. 4900(2002), 1187-1196
[12] Osten, W.; Seebacher, S.; Jüptner, W.: The application of Digital Holography for the inspection of microcomponents. Proc. SPIE Vol 4400, 2001, pp.1-15
[13] Seebacher, S.; Osten, W.; Baumbach, Th.; Jüptner, W.: The Determination of Material Parameters of Microcomponents Using Digital Holography. Opt. Las Eng. 36(2001)2, 103-126
[14] Osten, W. (Ed.): Optical Inspection of Microsystems. CRC Taylor & Francis, Boca Raton 2006
[15] Kujawinska M., et al.: "Calibration and assessment of full-field optical strain measurement procedures and instrumentation", Proc. SPIE Vol. 6341 (2006), 63410Q
[16] Pedrini, G.; Gaspar, J.; Osten, W.: Development of reference standards for the calibration of optical systems used in the measurement of microcomponents. Strain 46(2010)1, 79-88
[17] Pedrini, G.; Gaspar, J., Schmidt, M.; Alexeenko, I.; Paul, O.; Osten, W.: Measurement of nano/micro out-of-plane and in-plane displacements of micromechanical components by using digital holography and speckle interferometry. Opt. Eng. 2011, to be published
[18] Pedrini, G.; Gaspar, J.; Wu, T.; Paul, O.; Osten, W.: Calibration of optical systems for the measurement of microcomponents. Opt. & Las. Eng. 47(2009)2, pp. 203-210
[19] Wagner, C.; Osten, W.; Seebacher, S.: **„**Direct shape measurement by digital wavefront reconstruction and multi-wavelength contouring,“ Opt. Eng. 39(2000)1, 79-85
[20] Jüptner, W.; Kujawinska, M.; Osten, W.; Salbut, L.; Seebacher, S.: Combined measurement of silicon microbeams by grating interferometry and digital holography, Proc. SPIE Vol. 3407, pp. 348-357, 1998
[21] Yamaguchi, I.; Saito, H.: Application of holographic interferometry to the measurement of poisson´s ratio, Jap. Journal of Appl. Phys. 8, pp. 768-771, 1969

[22] Osten, W.; Jüptner, W.; Seebacher, S.; Baumbach, T.: The qualification of optical measurement techniques for the investigation of material parameters of microcomponents, Proc. SPIE Vol. 3825, 1999, pp. 152-164
[23] Seebacher, S.; Baumbach, Th.; Osten, W.; Jüptner, W.: Combined measurement of shape and deformation of small objects using digital holographic contouring and holographic interferometry. In: Rastogi, P. (Ed.): Proc. Int. Conf. On Trends in Optical Nondestructive Testing, Lugano 2000, pp. 55-65
[24] Birnbaum, G.; Vest, C. M., „Holographic nondestructive evaluation: status and future," Int. Adv. in Nondestr. Test 9(1983), 257-282
[25] Glünder, H.; and Lenz, R.: „Fault detection in nondestructive testing by an opto-electronic hybrid processor," Proc. SPIE Vol. 370(1982), pp. 157-162
[26] Robinson, D.W., „Automatic fringe analysis with a computer image processing system," Appl. Opt. 22(1983)14, 2169-2176
[27] Osten, W., Saedler, J., and Wilhelmi, W., „Fast evaluation of fringe patterns with a digital image processing system," (in German), Laser Magazin 2(1987), pp.58-66
[28] Jüptner, W., „Nondestructive Testing with Interferometry," Proc. Fringe´93, Akademie Verlag, Berlin, 1993, pp. 315-324
[29] Osten, W., Jüptner, W., and Mieth, U, „Knowledge assisted evaluation of fringe patterns for automatic fault detection," Proc. SPIE Vol. 2004(1993), pp. 256-268
[30] Jüptner, W., Kreis, T., Mieth, U., and Osten, W., „Application of neural networks and knowledge based systems for automatic identification of fault indicating fringe patterns," Proc. SPIE Interferometry´94 Vol. 2342(1994), pp. 16-26
[31] Osten, W.; Elandaloussi, F., and Jüptner, W., „Recognition by synthesis - a new approach for the recognition of material faults in HNDE," Proc. SPIE Vol. 2861(1996), 220-224
[32] Mieth, U.; W. Osten, W. Jüptner: Investigations on the appearance of material faults in holographic interferograms. Proc. Fringe 2001, Elsevier Sc. 2001, pp. 163-172
[33] Liedtke, C.E., "Intelligent Approaches in Image Analysis," In: Kujawinska M., Brown G., and Takeda M. (Eds.), Laser Interferometry IX: Techniques and Analysis, Proc. SPIE, Vol. 3478, pp. 2-10, Bellingham, 1998
[34] Elandaloussi, F., Osten, W., and Jüptner; W., "Automatic flaw detection using recognition by synthesis: Practical results," Proc. SPIE Vol. 3479(1998), pp. 228-234
[35] Merz, T., Elandaloussi, F., Osten, W., and Paulus, D., "Active approach for holographic nondestructive testing of satellite fuel tanks," Proc. SPIE Vol. 3824, 1999, pp.8-19
[36] Elandaloussi, F., Osten, W., and Jüptner, W., "Detektion und Analyse von Materialfehlern nach dem Prinzip Erkennung durch Synthese," Technisches Messen 5(2002), pp. 227-235
[37] Osten, W.: Holography and virtual 3D-Testing. In: *Proceedings of the1st International Berlin Workshop HoloMet 2000,* 14-17
[38] Osten, W.; Baumbach, T.; Jüptner, W.: A new sensor for remote interferometry. Proc. SPIE Vol. 4596(2001)158-168
[39] Osten, W.; Baumbach, Th.; Jüptner, W.: Comparative Digital Holography. Optics Letters, 27(2002)20, 1764-1766
[40] Baumbach, T.; Osten, W.; Kopylow, C.; Jüptner, W.: Remote metrology by comparative digital holography. Appl. Opt. 45(2006)5, 925-934
[41] Jeschke, S. et al: Networking Resources for Research and Scientific Education in BW-eLabs. Automation, Communication and Cybernetics in Science and Engineering 2009/2010, 2, pp. 241-258.
[42] Wilke, M., Alekseenko, I.; Situ, G.; Sarker, K.; Riedel, M.; Pedrini G.; Osten, W.: Remote Laboratory for Digital Holographic Metrology. Proc. SPIE Vol. 8082(2011), to be published
[43] Razum, M.: eSciDoc Infrastructure: A Fedora-Based e-Research Framework. ECDL, 5, 2009
[44] Selmer, A.: Weblabs in chemical engineering education. Trans. IChemE Part D, 2(2007), 38

Applied Mechanics and Materials Vol. 70 (2011) pp 21-27

doi:10.4028/www.scientific.net/AMM.70.21

Application of 3D Traction Force Microscopy to Mechanotransduction of Cell Clusters

Jacob Notbohm[1,a], Jin-Hong Kim[2,b],
Anand Asthagiri[3,c], and Guruswami Ravichandran[1,d]

[1]Division of Engineering and Applied Science, California Institute of Technology, 1200 East California Boulevard, MC 105-50, Pasadena, CA 91125, USA

[2]Cell Dynamics Research Center, Gwangju Institute of Science and Technology, South Korea

[3]Department of Chemical Engineering, Northeastern University, Boston, MA 02115, USA

[a]notbohm@caltech.edu, [b]jinkim11@gmail.com, [c]a.asthagiri@neu.edu, [d]ravi@caltech.edu

Keywords: 3D traction force microscopy, mechanotransduction, digital volume correlation

Abstract. With increasing understanding of the important role mechanics plays in cell behavior, the experimental technique of traction force microscopy has grown in popularity over the past decade. While researchers have assumed that cells on a flat substrate apply tractions in only two dimensions, a finite element simulation is discussed here that demonstrates how cells apply tractions in all three dimensions. Three dimensional traction force microscopy is then used to experimentally confirm the finite element results. Finally, the implications that the traction distributions of cell clusters have on the study of inhibition of proliferation due to cell contact and scattering of cells in a cluster are discussed.

Introduction

The mechanical behavior of cells has been shown to affect cell adhesion, growth, differentiation [1], and migration [2]. In addition, researchers are studying the relationship between cell mechanics and cancer metastasis [3], morphogenesis, and wound healing. The vast range of applications related to cell mechanics indicates that there is a need for analytical, numerical, and experimental work in the fundamental area of cell mechanics.

The technique of traction force microscopy (TFM) offers a way to passively measure the mechanical processes of cell locomotion [4,5], cell communication [6], and cell-cell adhesion [7]. In the TFM technique, a cell is placed onto a flat substrate, and the tractions applied by the cell are inferred by measuring the displacements of the substrate by tracking the motion of markers within the substrate. Nearly all previous studies have measured only the two-dimensional (2D), in-plane displacements of the substrate, and some studies have even argued that a cell can only apply forces in two dimensions [5,8]. However, a thought experiment on the application of contractile forces by a cell on a flat substrate would seem to imply that cells do apply forces in three dimensions. Additionally, two recent studies have proven that cells apply tractions in all three dimensions [9,10].

Most previous TFM experiments have been performed on single cells. However, multicellular assembly of cells is a mechanical process as well: it involves adhesion of individual cells to the underlying substrate and their neighbors. For these cells to adhere, mechanical forces must be present. Therefore, using TFM to study how cell clusters apply forces to the substrate beneath them and to their neighbors is of current interest. Previous research has shown that cell proliferation is increased when cells exert higher traction forces [11], and that higher traction forces lead to cell scattering in a process similar to epithelial-mesenchymal transition [12]. Despite these observations, the underlying mechanisms that cause cells to respond to mechanical force are still not well understood. Thus, we study the traction distribution applied by epithelial cells in a cluster. We use the observation that a monolayer of epithelial cells grown on a soft substratum undergo contact inhibition wherein cell cycle activity of interior cells ceases while peripheral cells continue to divide. Because cells transduce mechanical force to each other intercellularly, there is a competition of cell - generated contractile forces between cell - cell and cell - matrix adhesions. We hypothesize that interior cells, having a relatively high amount of cell - cell contact, rely less on the underlying substrate and therefore apply smaller traction forces to the surface beneath them than peripheral cells do.

In this paper, we discuss a simple finite element model that demonstrates how cells can apply forces in all three dimensions, even when placed on a flat surface. We then compare this model to experimental data collected using three-dimensional (3D) TFM on Madin Darby canine kidney cell clusters. Finally, we discuss the implications of the traction data on the study of mechanotransduction by suggesting ways in which tractions affect processes such as cell scattering and cell contact inhibition.

Methods

Finite Element Model. In order to develop an intuitive understanding for why a cell on a planar substrate would apply tractions in all three dimensions, a simple finite element model of the geometry is created in ABAQUS 6.9 (Simulia, Providence, RI). In the model, the substrate properties are chosen such that they match the properties of the polyacrylamide gels that are used as substrates in the experiments: the substrate is modeled with linear elastic 8-node bricks with Young's modulus of 7.1 kPa and Poisson's ratio of 0.48. The cells are also modeled as linear elastic 8-node bricks with Young's modulus 1 kPa and Poisson's ratio 0.48. The cell elements are connected to the substrate by tying the nodes at the exterior of the cells to the substrate. In-plane contraction of the cells is modeled using a thermal strain in the cell elements. Since a cell on a substrate probably contracts the most in the in-plane (2D) directions, the thermal contraction is applied only in the in-plane directions.

Two different problems are modeled here: a single cell (18x18 μm^2) on a substrate, and a cell cluster (90x90 μm^2, 25 cells) on a substrate. The substrate is 75 μm thick, which closely matches the substrate thickness of the experiments. The in-plane dimensions of the substrate are 150x150 μm^2, which is assumed to be large enough to be essentially infinite for this simple study. Symmetry boundary conditions are used on the front and left faces of the model, and a fixed boundary condition is used at the bottom of the substrate. A sketch of the model is shown in figure 1.

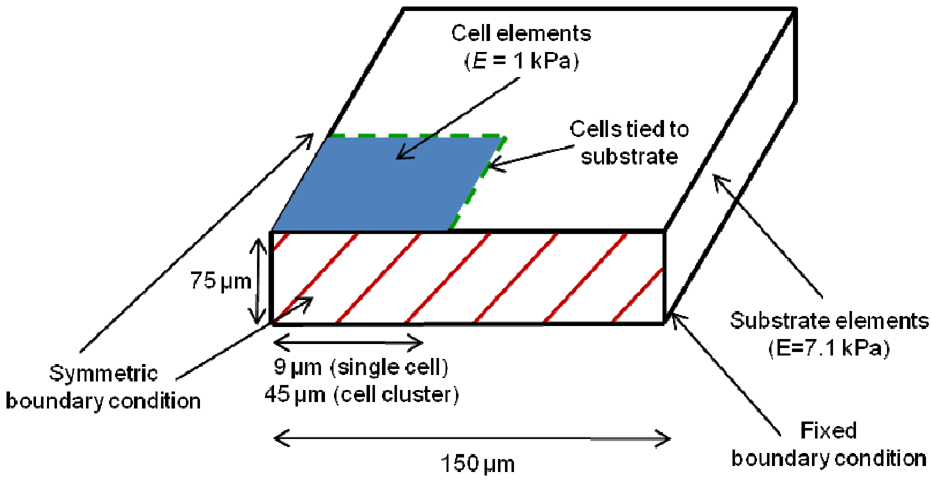

Figure 1: The model used in the finite element simulations. Cell and substrate elements are linear elastic 8-node bricks. Symmetric boundary conditions are used on the front and left faces of the model; a fixed boundary is applied to the bottom of the substrate. Exterior cell nodes are tied to the substrate.

Cell culture. Madin Darby canine kidney cells were grown in Dulbecco's modified Eagle's medium with HEPES and L-glutamine (Invitrogen, Carlsbad, CA) and 10% (v/v) fetal bovine serum (Invitrogen). Prior to experiments, cells were placed in serum-starved medium for 24 hours and then stained with Mitotracker Deep Red (Invitrogen) for imaging.

Preparation of Polyacrylamide Gels. Polyacrylamide gels are used as the substrate in the TFM experiments. The gels are made with 40% stock solution polyacrylamide (Bio-Rad, Hercules, CA) and 2% stock solution bisacrylamide (Bio-Rad) and are mixed with deionized water to a concentration of 10% polyacrylamide and 0.04% bisacrylaimde. 1 μm fluorescent microbeads (Invitrogen) are suspended in the gels at a concentration of approximately 0.2%, and the gels are pipetted onto a 25 mm glass coverslip. A 15 mm glass coverslip is placed onto the gel before it polymerizes, creating a polyacrylamide film with a thickness of 75 μm.

The 15 mm coverglass is then removed, and the polyacrylamide gels are functionalized with fibronectin (Sigma-Aldrich, St. Louis, MO) using the heterobifunctional cross-linker sulfo-SANPAH (Pierce) as described previously [13]. The Young's modulus of the gels was determined by using a custom-built compression experiment to perform stress-relaxation tests on the gels, as described previously [14]. It was found that the Young's modulus of the gels was 7.1±0.4 kPa. This gel stiffness was chosen, because it was the smallest stiffness that allowed the cells to spread onto the gel in a monolayer; more compliant gels caused the cells to clump up onto each other.

Confocal Microscopy. A Nikon C1 confocal microscope on a TE2000 stand is used with a 40x 0.6 NA air objective. A 488 nm argon laser and a 633 nm helium-neon laser are used to excite fluorescence. 512x512 pixel images are collected in a field of view of 150x150 μm^2. A 32 μm confocal stack is collected with a step size of 0.4 μm. Then the cells are lysed with 0.5% Triton X-100 (Invitrogen), and a second volume stack is collected. A diagram of the experimental setup is shown in figure 2. All confocal imaging is performed at 37°C using a custom-build enclosure heated with an Air Therm ATX heater (World Precision Instruments, Sarasota, FL). Control experiments are performed wherein a polyacrylamide gel with no cells is imaged before and after injecting Triton, and displacements were found to be approximately 0.02 μm using DVC (discussed below).

Digital Volume Correlation and Traction Calculation. To calculate the displacements, strains, and stresses applied by the MDCK cell clusters to the polyacrylamide substrate, a digital volume correlation (DVC) algorithm [14] is used to calculate the full 3D displacement profile within the

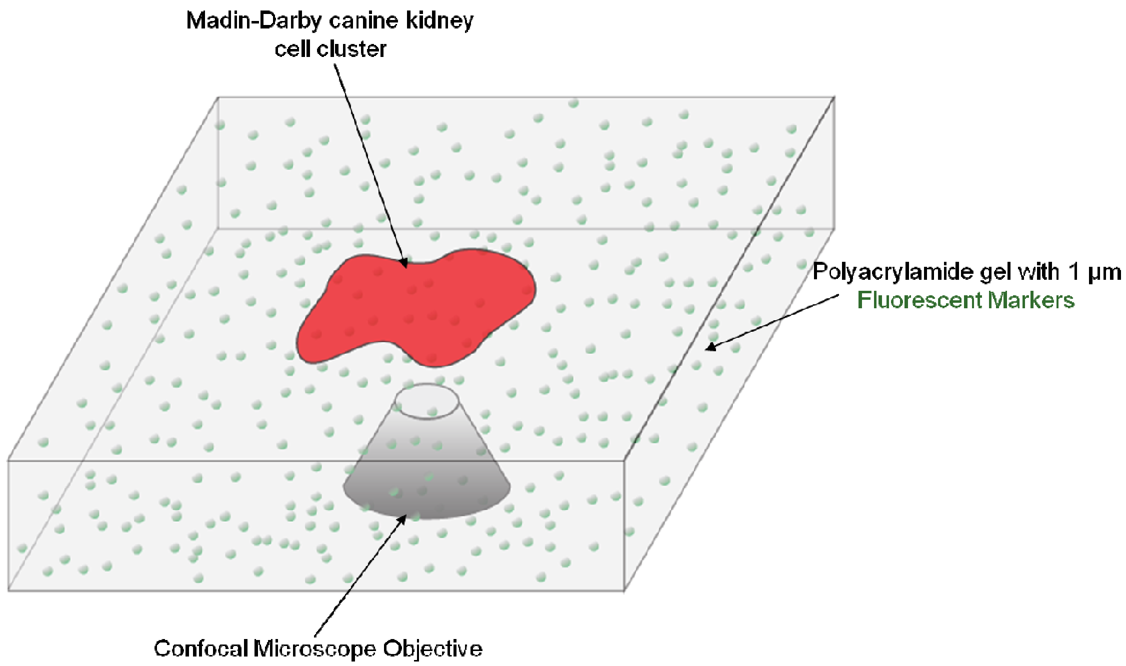

Figure 2: A diagram of the experimental protocol.

substrate. Briefly, this algorithm labels the intensity distribution of 64x64x64 voxel subset as $f(\boldsymbol{x})$. It is assumed between the reference and deformed images that the subset undergoes a rigid body translation with mapping $\boldsymbol{y}=\boldsymbol{x}+\boldsymbol{c}$. By using this mapping along with the intensity distribution of the deformed image $g(\boldsymbol{y})$, the DVC algorithm solves the equation $f(\boldsymbol{x})=g(\boldsymbol{y})=g(\boldsymbol{x}+\boldsymbol{c})$ for $\boldsymbol{c}$, which corresponds to the 3D displacement vector of the subset of interest. The DVC algorithm then moves on to another subset and repeats this process. While the subsets could be separated from each other by as small as one pixel, such fine resolution is computationally expensive, so a subset separation of 8 pixels is used here.

The use of a volume correlation algorithm offers multiple advantages over tracking the displacement of multiple individual particles. The first advantage of the correlation algorithm is that displacements are calculated on a regular set of grid points, which facilitates the computation of strain. The second advantage of volume correlation is that a denser concentration of fluorescent microbeads may be used, since individual particles do not have to be followed during deformation. Finally, the volume correlation algorithm uses more data in the computation of the displacements of each subset (64x64x64 voxels are used here, as opposed to the intensity of a single particle), which can give better resolution: some authors report that image correlation can achieve a displacement resolution of 0.02 pixels [15].

After displacement computation, the displacements are filtered with a low pass filter. Strains are calculated from the filtered displacement data by fitting a 3x3x3 window of grid points to a tri-linear function to determine the displacement gradients. Once the strain tensor is assembled, the stress tensor is computed from the incompressible Hooke's law, $\boldsymbol{\sigma}=2\mu\boldsymbol{\varepsilon}$ where μ is the shear modulus, and the stress tensor is again filtered with a low pass filter. The tractions applied by the cell cluster to the substrate are calculated according to the Cauchy relation, $\boldsymbol{t}=\boldsymbol{\sigma}\cdot\boldsymbol{n}$, where $\boldsymbol{t}$ is the traction vector, and $\boldsymbol{n}$ is the unit vector normal to the substrate surface.

Results

Finite Element Simulations. A finite element model is created to better understand the way in which a contractile cell or cell cluster applies force to a flat susbstrate beneath it. In the simulation, cell contraction is modeled by applying equibiaxial strain to the substrate through an in-plane thermal contraction. Figure 3 shows plots of the traction magnitudes and individual traction components applied by the cells to the substrate. Inspection of the plots of individual traction components shows that the traction components in the z direction have the same magnitude and are sometimes larger than the traction components in the in-plane (x and y) directions. While it is expected that in-plane contraction of the cell cluster would cause displacements in the z direction as a result of the Poisson effect within the substrate, it may be a surprise that tractions in the z direction also exist. These tractions result from a bending deformation of the contractile (cell) layer, which pushes the interior of each cell downward. To maintain force equilibrium in the contractile layer, the exterior of each cell pulls upward on the substrate.

Traction Force Microscopy Experiments. Several 3D TFM experiments were performed wherein the 3D tractions applied by the MDCK cell clusters to the substrate were calculated from measurements of bead displacements. Characteristic data from this experiment is shown in figure 4. The plots of individual traction vector components in figure 4 clearly show that cell clusters apply tractions in all three dimensions, which agrees with previous findings for single cells [9,10]. The data shows that the cell cluster pulls inward on the polyacrylamide substrate. Additionally, the exterior cells pull the substrate upward.

Discussion

In a cultured cell cluster, cells adhere both to each other and to the substrate beneath them. The contour plot in figure 4a shows that these cells seem to apply tractions primarily at the outside of the cluster, indicating that interior cells do not apply force to the substrate in the same way that

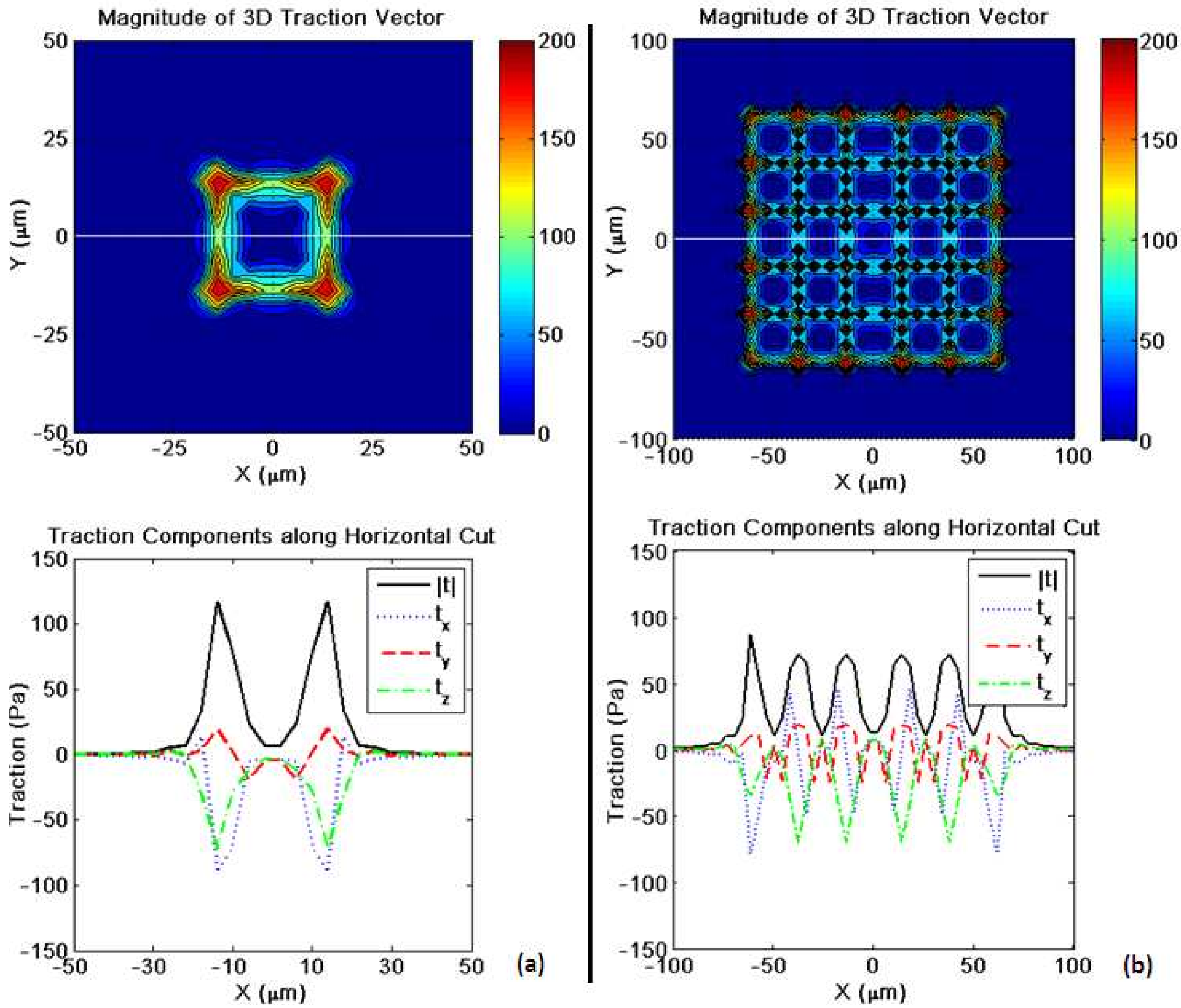

Figure 3: Results of the finite element model, which simulates contraction of a single cell (a) and a cell cluster (b). Contour plots show the magnitude of the 3D traction vector (units: Pa). Line plots show the individual traction components along the horizontal cuts shown in white on the contour plots.

exterior cells do. As mentioned previously, the substrate stiffness of 7.1 kPa is chosen, because this is the most compliant substrate that allows the cells to form a monolayer. This observation along with the TFM data leads to the hypothesis that on this substrate, interior cells form stronger cell-cell adhesions than exterior cells. Therefore, the forces applied by interior cells are applied primarily to neighboring cells, which the forces applied by exterior cells are applied to the substrate. Such a hypothesis would have interesting consequences to our understanding of contact inhibition of cell proliferation and cell scattering. Contact inhibition and scattering have been shown to have chemical cues such as growth factors [16], but we suggest that mechanical cues are likely present as well. We are currently studying this hypothesis by investigating how cells respond to mechanical cues such as substrates of different stiffness and to chemical cues such as epidermal growth factor.

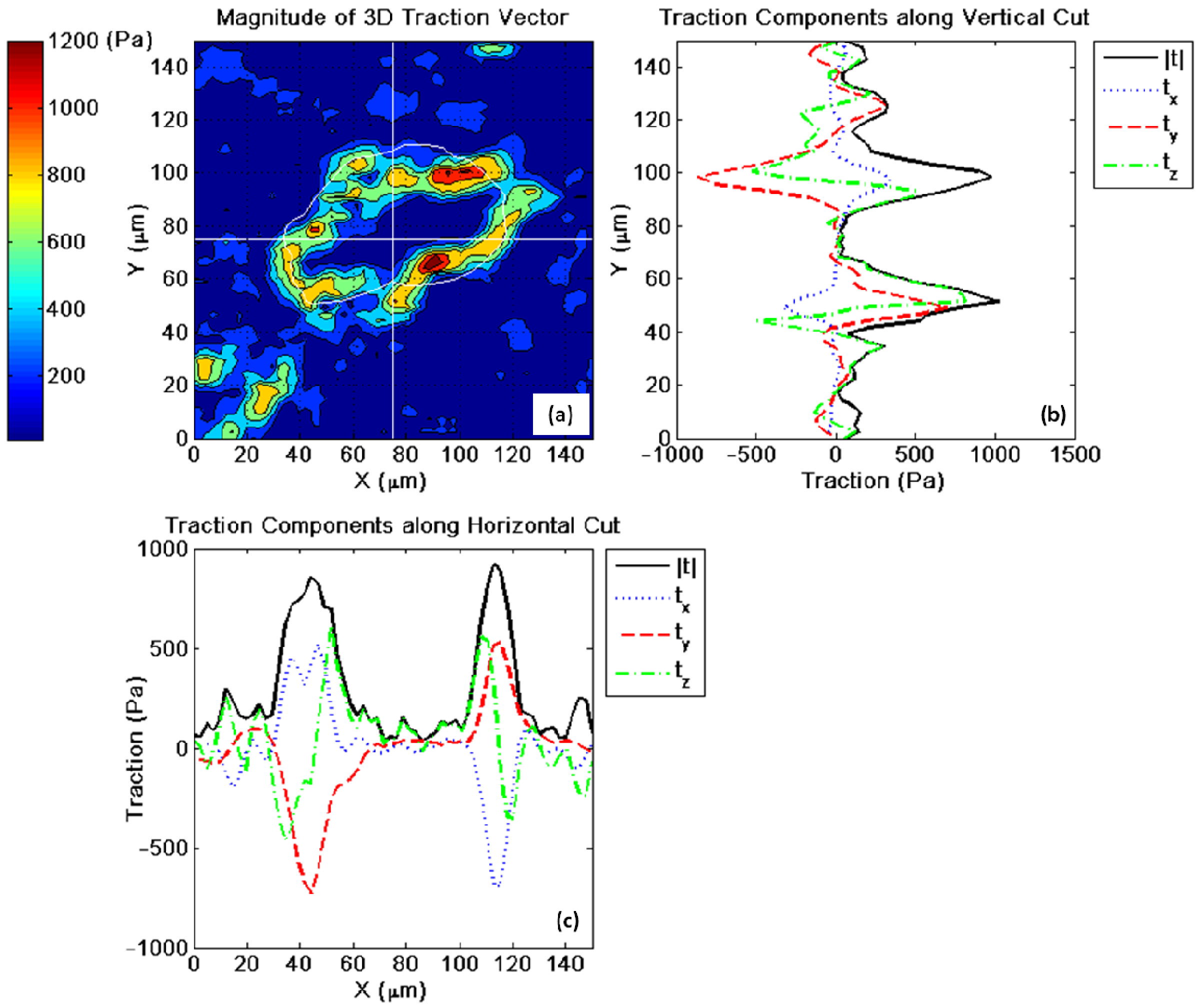

Figure 4: Tractions applied by a MDCK cell cluster on a polyacrylamide substrate. Traction magnitudes are shown in (a) with an outline showing the location of the cell cluster. Individual traction components along the vertical and horizontal cuts in the contour plot are shown in (b) and (c) respectively.

Conclusions

A key finding in this study is that both single cells and cell clusters apply tractions to a flat substrate in all three dimensions. This result highlights the need for use of 3D techniques to fully characterize the way in which a cell interacts with its surroundings. While many studies using TFM have focused primarily on single cells, this study considers the way in which a cluster of cells applies tractions to the substrate beneath them. The application of 3D TFM to the study of cell clusters demonstrates the versatility of the technique of 3D TFM, and it is leading to an understanding of the mechanical cues involved in interaction of cells such as contact inhibition and cell scattering.

Acknowledgments

We thank Christian Franck, Stacey Maskarinec, and David Tirrell for their contributions towards developing the DVC and traction calculation techniques. This work was funded by a grant from the National Science Foundation through the Center for the Science and Engineering of Materials at the California Institute of Technology. J.N. was supported by the United States Department of Defense through the National Defense Science & Engineering Graduate Fellowship Program. J.H.K. was supported the NCI-USC Physical Sciences of Oncology Center (U54CA143907).

References

[1] D.E. Discher, P. Janmey, and Y.L. Wang: Science Vol. 310 (2005), p. 1139.

[2] T. Oliver, M. Dembo, and K. Jacobson: Journal of Cell Biology Vol. 145 (1999), p. 589.

[3] S. Suresh: Acta Biomaterialia Vol. 3 (2007), p. 3989.

[4] T. Oliver, M. Dembo, and K. Jacobson: Cell Motility and the Cytoskeleton Vol. 31 (1995), p. 225.

[5] M. Dembo and Y.L. Wang: Biophys J Vol. 76 (1999), p. 2307.

[6] C.A. Reinhart-King, M. Dembo, and D.A. Hammer: Biophs J Vol. 95 (2008), p. 6044.

[7] X. Trepat, M.R.Wasserman, T.E. Angelini, E. Millet, D.A.Weitz, J. P. Butler, and J.J. Fredberg: Nature Physics Vol. 5 (2009), p. 426.

[8] B. Sabass, M.L. Gardel, C.M. Waterman, and U.S. Schwarz: Biophys J Vol. 94 (2008), p. 207.

[9] S.A. Maskarinec, C. Franck, D.A. Tirrell, and G. Ravichandran: Proc. Nat. Acad. Sci. USA Vol. 106 (2009), p. 22108.

[10] S.S. Hur, Y. Zhao, Y.S. Li, E. Botvinick, and S. Chien: Cellular and Molecular Bioeng. Vol. 2 (2009), p. 425.

[11] C.M. Nelson, R.P. Jean, J.L. Tan, W.F. Liu, N.J. Sniadecki, A.A. Spector, and C.S. Chen: Proc. Nat. Acad. Sci. USA Vol. 102 (2005), p. 11594.

[12] J. de Rooij, A. Kerstens, G. Danuser, M.A. Schwartz, and C.M. Waterman-Storer: Journal of Cell Biology Vol. 171 (2005), p. 153.

[13] R.J. Pelham and Y.L. Wang: Proc. Natl. Acad. Sci. USA Vol. 94 (1997), p. 13661.

[14] C. Franck, S. Hong, S.A. Maskarinec, D.A. Tirrell, and G. Ravichandran: Experimental Mechanics Vol. 47 (2007), p. 427.

[15] J.W. Dally and W.F. Riley: *Experimental Stress Analysis*, 4th ed. (College House Enterprises, Knoxville, TN 2005).

[16] J.H. Kim, K. Kushiro, N.A. Graham, and A.R. Asthagiri: Proc. Natl. Acad. Sci. USA Vol. 106 (2009) p. 11149.

Applied Mechanics and Materials Vol. 70 (2011) pp 28-32
© (2011) Trans Tech Publications, Switzerland
doi:10.4028/www.scientific.net/AMM.70.28

Measurement of Thermomechanical Coupling and Its Application in Stress and Damage Analysis

J. M. Dulieu-Barton

School of Engineering Science, University of Southampton, Highfield, Southampton, SO17 1BJ, UK

janice@soton.ac.uk

Keywords: TSA, Infra-red thermography, Composites

Abstract.

Polymer composites are increasingly being used in high-end and military applications, mainly due to their excellent tailorability to specific loading scenarios and strength/stiffness to weight ratios. The overall purpose of the ongoing research at the University of Southampton is to develop an enhanced understanding of the behaviour of fibre reinforced polymer composites when subjected to a range of loading scenarios. The measurements lecture reviews progress in using the thermoelastic stress analysis technique as a tool that enables a better understanding of the behaviour of polymer composite single skin and sandwich structures.

Introduction

The relationship between mechanical deformation and thermal energy in an elastic solid is known as the thermoelastic effect [1]. By assuming isentropic behaviour and neglecting the temperature dependence of the elastic constants it can be shown that for a linear elastic, homogenous material the rate of change of temperature is a function of the applied stresses as follows [2]:

$$\Delta T = -\frac{\alpha T_0}{\rho C_p}\Delta(\sigma_1 + \sigma_2) \quad (1)$$

where T is the temperature, T_0 is the absolute (reference) temperature, C_p is the specific heat at constant strain, α is the coefficient linear thermal expansion, ρ is the mass density, σ is the direct stress and the subscripts 1 and 2 can denote principal values.

In the past three decades the experimental technique known as ***thermoelastic stress analysis (TSA)*** has been developed. The technique is based on the measurement of the small temperature change given in equation (1) by means of an infra-red detector. Until recently it was necessary to use detectors that were not radiometrically calibrated so the working equation was defined in terms of the digital level output from the detector known as the ***thermoelastic signal*** [2]. The well-known equation that related the thermoelastic signal, S, to the stresses was first suggested by Stanley and Chan in 1985 [2] in the following form:

$$S = \Delta\left(\sigma_1 + \sigma_2\right) / A \quad (2)$$

where A is a calibration constant that takes into account the specimen material properties and the detector properties. However the calibration constant must be defined for any given surface temperature, as the detector has a very strong dependence on surface temperature particularly for the detectors that operate on the 2 -5 μm wavelength range [3]. Equation (2) has been used as the basis for numerous studies spanning almost three decades. Since the initial validation in [2], it has been demonstrated that the approach can be used in a wide range of applications and that the calibration constant can be evaluated in a straightforward manner [4]. With more modern radiometrically calibrated detectors it is possible to derive ΔT 'directly'. Here identical approaches to those suggested in [4] can be used to find the thermoelastic constant K. A known stress is applied to a specimen ΔT and T are obtained from the measurement and therefore K is obtained.

The greatest inaccuracies in TSA occur when ΔT does not occur adiabatically. For a general test specimen it is impossible to achieve fully adiabatic conditions experimentally; however, for the purposes of TSA a *pseudo-adiabatic* state may be achieved, where there is no measurable attenuation of the thermoelastic signal due to heat transfer. The usual approach is to cyclically load the specimen, so that the rate of change of the stress is large, compared to spatial changes in the stress across a projected element of the infra-red detector. However, in many cases, particularly in small specimens, where stress gradients are high this can be difficult to achieve [5]. Furthermore, if the specimen is coated with paint there is a step change in the thermal characteristics at the interface and this too causes non adiabatic behaviour. In polymer composite materials these two difficulties can be avoided and usually the material thermal conductivity is low and often as the emissivity of polymer resins is high it is not necessary to use a paint coating [6].

The purpose of the current paper is to show how the thermomechanical coupling, which results in the thermoelastic effect can be used in a wide range of studies including damage analysis of composite structures and finite element analysis validations of composite structures. The paper finishes with a look into the future, discussing the possibilities of using transient loading, instead of cyclic loading to create a strain based non-destructive evaluation tool.

Composite materials

The simple thermoelastic theory devised for an isotropic body in equation (1) is not valid for orthotropic materials [7]. For orthotropic materials the following equation is used [7]:

$$\Delta T = -\frac{T}{\rho C_p}(\alpha_1 \Delta\sigma_1 + \alpha_2 \Delta\sigma_2) \tag{3}$$

where $\Delta\sigma$ is the change in the direct surface stress, A^* is a further calibration constant and the subscripts 1 and 2 denote the principal material directions of the surface lamina.

Stanley and Chan [7] validated equation (3) using two types of composite component. Potter [8] proposed a thermoelastic theory relating the thermoelastic output to that of the surface strains and demonstrated its validity on a carbon fibre / epoxy resin laminate. Bakis and Reifsnider [9] investigated the influence of material inhomogeneity and anisotropy using carbon fibre reinforced plastics. It was found that the thermoelastic response was affected by a number of factors, which included the volume fraction, the thermoelastic properties of the micro-constituent materials, the orientations of the laminae within the laminate, and the orientation of the lamina on the surface. Emery et al [10] suggested a method for establishing a general calibration approach for orthotropic composites and showed for the type of composite used the response was a function of the resin rich surface layer and that largely the orthotropic material response could be neglected. This has allowed for a certain class of material for the stress change to be decoupled from the material properties and for stresses to be evaluated. This has also been noted by other researchers, [11, 12]; however for the majority of cases where there is not a resin rich layer the bracket quantity in equation (3) does not provide the stresses. Moreover the bracketed quantity is a stress metric and therefore can be used as a tool for damage analysis and also for validation of finite element models. Some examples of the work conducted at the University of Southampton on both damage analysis and model validation are provided in the paper.

Damage studies

In [13] the generalised form of the thermoelastic equations presented in [10] is used as the basis for damage analysis. The thermoelastic response is expressed in terms of the change in laminate strains; the laminate strains can be measured in a simple tensile test and related to the thermoelastic signal, so that it is possible to group the material constants into a ‘calibration constant’ [10]. For the material used in the study, it has been shown that the thermoelastic response does not emanate from the orthotropic surface ply but from the isotropic resin-rich surface layer. The existence of the resin-rich layer considerably simplifies the analysis. The resin-rich layer renders the laminates ‘mechanically orthotropic’, but ‘thermoelastically isotropic’. This enabled a new calibration constant to be devised, B^*, as follows:

$$\frac{\Delta\varepsilon_L(1-\nu_{LT})}{S}=\frac{A^*(1-\nu_R)}{\alpha_R E_R}=B^* \tag{4}$$

where ν_R is the major Poisson’s ratio of the resin-rich layer, α_R is the coefficient of thermal expansion of the resin-rich layer, E_R is the Young’s modulus of the resin-rich layer, ν_{LT} is the major Poisson’s ratio of the laminate, A^* is a calibration constant and S is the thermoelastic signal, i.e. the digitized output from the IR detector.

The damage analysis procedure was implemented using a MATLAB program that is applied to the data array obtained from the infra-red system and presented the output in a full-field manner. It incorporates both the temperature correction procedure [3] and the strain calibration procedure [10]. Firstly thermoelastic data, S_0, and absolute temperature, T_0, were obtained from the undamaged specimens. The S_0 data was used to obtain the calibration constant B^* and the T_0 data was used as the baseline for the temperature correction. A damaging load was applied to the specimen and thermoelastic data, S_m, and the temperature, T_m, are obtained at various stages throughout the component life. A data set was obtained that was temperature corrected in a point-by-point fashion. The resulting output from this, S_c, was then calibrated, so that a metric was obtained that provided the strain sum change in the damaged component, which occurred purely as a result of the stress redistribution in the component. The methodology was demonstrated in cross-ply and quasi-isotropic laminate strips that contained a circular hole. It was shown that the maximum strain change obtained from the full field thermoelastic data indicated clearly the inception of cracking and delamination.

A different approach was used in [14] for woven laminates here rather than calibrate the response a metric of the difference $\Delta T/T$ from undamaged to damaged states was used. It was shown that the thermoelastic response could reveal cracks in the yarns transverse to the loading direction at very low levels of fatigue loading.

Validation of finite element models

In composite structures the stress distributions are complex and dependent not only upon the line of action of the applied load but the material orientation as well. Numerical modelling of the stresses in such structures is not a straightforward proposition, particularly for inhomogeneous laminated structures whose behaviour may be governed by both geometric and material nonlinearities. In the late 1990s [15,16], a methodology was proposed to provide a finite element model validation procedure based on TSA. The ideas were demonstrated on single skin and sandwich tee-joints. The premise was simple, to make the finite element data into the same form as the thermoelastic data. It is possible to combine the material constants in the principal material directions, e.g.. α_x, α_y, ρ and C_p into two thermoelastic constants K_x and K_y as follows:

$$\Delta T=-T\left(K_x\sigma_x+K_y\sigma_y\right) \tag{5}$$

where $K_x=\dfrac{\alpha_x}{\rho C_p}$ and $K_y=\dfrac{\alpha_y}{\rho C_p}$.

Equation (5) can be rearranged so that a stress metric is obtained where the measured ΔT can be calibrated in such a way that it can be used for finite element analysis validation:

$$\underbrace{\frac{\Delta T}{TK_x}}_{TSA} = \underbrace{\Delta\sigma_x + \frac{K_y}{K_x}\Delta\sigma_y}_{FE} \qquad (6)$$

The left hand side of Equation (6) represents the calibration of ΔT into a stress metric and the right hand side into the form that the finite element data must be processed to make it comparable with the TSA data. Therefore an experimental means of deriving the thermoelastic constants was established. Since the initial work the approach has proved successful on adhesively bonded joints [17] and sandwich panels [18].

Transient loading

The modern infrared (IR) detectors that are used to measure this temperature change in TSA are compact, robust systems that operate in conjunction with a standard PC. The technique therefore offers great potential as a non-destructive strain-based damage assessment tool, which could be used to assess components during routine inspections in the field. However, the current methodology presents a barrier that has hitherto tethered to the technique to laboratory testing only. It is the requirement for a controlled cyclic load and corresponding reference signal that presents a barrier to moving the technique from the laboratory into the field, significantly constraining its application range. Recent work [19] has initiated a modified approach to TSA that circumvents this barrier. In the proposed new TSA methodology, the component under test is subjected to a single transient load. In [19] two methods of imparting the transient load into fibre reinforced polymer composite specimens were defined, and underpinned the new methodology. The results from the new approach were then validated using both theory and the standard TSA method. Finally the potential of the new TSA methodology was demonstrated through application to the assessment of damage growth in three different polymer composite laminates. Presently the ideas introduced in [19] are being developed in a programme funded by the MATERA + EU action and it is envisaged that in the future TSA will be used as a strain based non-destructive evaluation technique.

Conclusions

The lecture has described in detail progress in evaluating composite structures using TSA. It has been shown how the thermomechanical coupling that enables the thermoelastic effect can be used in damage studies and finite element model validation of polymer composite structures. The potential of using TSA as a strain based non-destructive evaluation tool has been explored.

Acknowledgements

The author would like to acknowledge the support of her co-workers and students in the production of this chapter, in particular Dr Trystan Emery, Dr Richard Fruehmann, Dr Duncan Crump, Dr Jacqui Earl and Dr Simon Quinn. She is extremely grateful to her former PhD supervisor and co-worker Emeritus Professor Peter Stanley from the University of Manchester, who introduced her to the technique and provided unrelenting encouragement to build on the research conducted in the early 1990s in a small laboratory in Manchester.

References

[1] Thomson, W. On the thermoelastic properties of matter, Q.J. Maths. 1855, **I**, 57-77.

[2] Stanley P, Chan WK. Quantitative stress analysis by means of the thermoelastic effect. J Strain Anal Eng 1984; **20** (3):129-137

[3] Dulieu-Barton JM, Emery TR, Quinn S, Cunningham PR. A temperature correction methodology for quantitative thermoelastic stress analysis and damage assessment. Meas Sci Technol 2006; **17**(6): 1627-1637.

[4] Dulieu-Smith JM. Alternative calibration techniques for quantitative thermoelastic stress analysis. Strain 1995; **31**(1): 9-16.

[5] Wang WJ, Dulieu-Barton JM and Li Q. "Assessment of non-adiabatic behaviour in thermoelastic stress analysis of small scale components", Experimental Mechanics, 2010, 50, 449-461. DOI: 10.1007/s11340-009-9249-2.

[6] Robinson, AF., Dulieu-Barton, J.M., Quinn, S. and Burguete R.L., "Paint coating characterisation for thermoelastic stress analysis" Measurement Science and Technology, 2010, 21, 085502.

[7] Stanley P, Chan WK. The application of thermoelastic stress analysis to composite materials. J Strain Anal Eng 1988; **23**(3): 137-142.

[8] Potter RT. Stress analysis in laminated fibre composites by thermoelastic emission. In: Proceedings of the 2nd international conference on stress analysis by thermoelastic techniques, SPIE vol. 731, London, 1987

[9] Bakis CE, Reifsnider KL. The adiabatic thermoelastic effect in laminated fiber composites. J Compos Mater 1991; **25**: 809-830.

[10] Emery TR, Dulieu-Barton JM, Earl, JS and Cunningham, PR. A generalised approach to the calibration of orthotropic materials for thermoelastic stress analysis. Composites Science and Technology, 2008, **68**: 743-752.

[11] El-Hajjar R, Haj-Ali R. A quantitative thermoelastic stress analysis method for pultruded composites. Comp Sci Tech 2003; **63**(7): 967-978.

[12] Pitarresi G, Found MS, Patterson EA. An investigation of the influence of macroscopic heterogeneity on the thermoelastic response of fibre reinforced plastics. Comp Sci Tech 2005; **65**(2): 269-280.

[13] Emery TR and Dulieu-Barton JM. Thermoelastic Stress Analysis of damage mechanisms in composite materials. Composites Part A 2010; **41**: 1729-1742.

DOI: 10.1016/j.compositesa.2009.08.015.

[14] Fruehmann RK, Dulieu-Barton JM and Quinn, S. Assessment of fatigue damage evolution in woven composite materials using infra-red techniques. Composites Science and Technology 2010; **70**: 937-946. DOI: /10.1016/j.compscitech.2010.02.009

[15] Dulieu-Smith JM, Quinn S, Shenoi RA, Read PJCL, Moy SSJ. Thermoelastic stress analysis of a GRP tee joint. App Compos Mater 1997; **4**(5): 283-303.

[16] Dulieu-Barton JM, Earl JS, Shenoi RA. Determination of the stress distribution in foam-cored sandwich construction composite tee joints. J Strain Anal Eng 2001; **36**(6): 545-560.

[17] Boyd SW, Dulieu-Barton JM, Rumsey L. Stress analysis of finger joints in pultruded GRP material. Int J Adhes Adhes 2006; **26**(7): 498-510.

[18] Crump DA, Dulieu-Barton, J.M. and Savage, J. Design and commission of an experimental test rig to apply a full-scale pressure load on composite sandwich panels representative of aircraft secondary structure. Measurement Science and Technology, 2010; **21** 16pp 015108.

[19] Fruehmann RK, Dulieu-Barton JM and Quinn S. Thermoelastic stress and damage analysis using transient loading. Experimental Mechanics 2010; **50**, 1075-1086.

Applied Mechanics and Materials Vol. 70 (2011) pp 33-38
© (2011) Trans Tech Publications, Switzerland
doi:10.4028/www.scientific.net/AMM.70.33

The development of a reference material for calibration of full-field optical measurement systems for dynamic deformation measurements

Andrea Davighi[1,a], Richard Burguete[2,b], Mara Feligiotti[3,c], Erwin Hack[3,d], Simon James[4,e], Eann Patterson[5,f], Thorsten Siebert[6,g], Maurice Whelan[1,h]

[1]Institute for Health and Consumer Protection, European Commission DG Joint Research Centre, 21027, Ispra (VA), Italy.

[2]Airbus, New Filton House, Filton, Bristol BS99 7AR, UK.

[3]EMPA, Swiss Federal Laboratories for Materials Science and Technology, Laboratory for Electronics/Metrology/Reliability, CH-8600 Dübendorf, Switzerland.

[4]School of Engineering, The University of Liverpool, The Quadrangle, Liverpool L69 3GH, UK.

[5]Composite Vehicle Research Center, Michigan State University, East Lansing, MI, USA

[6]Dantec Dynamics GmbH, Kaessbohrer Str. 18, D 89077 Ulm, Germany.

[a]andrea.davighi@jrc.ec.europa.eu, [b]richard.burguete@airbus.com, [c]mara.feligiotti@empa.ch, [d]erwin.hack@empa.ch, [e]Simon.James@liverpool.ac.uk, [f]eann@egr.msu.edu, [g]thorsten.siebert@dantecdynamics.com, [h]maurice.whelan@ec.europa.eu

Keywords: calibration, international standard, optical method for measurements.

Abstract.
A reference material is defined as material, sufficiently homogeneous and stable with respect to one or more specified properties, which has been established to be fit for its intended use in a measurement process. Reference materials provide a simple definition of the measured quantity that can be traced to an international standard and can be used to assess the uncertainty associated with a measurement system. Previous work established a reference material and procedure for calibrating full-field optical systems suitable for measuring static, in-plane strain distributions. Efforts are now underway to extend this work to the calibration of systems capable of measuring three-dimensional deformation fields induced by dynamic loading. The important attributes for a dynamic reference material have been identified in a systematic and rational fashion, which have been subsequently translated into a generic design specification. Initial prototypes of candidate designs have been produced and evaluated using experimental modal analysis and digital speckle interferometry, and the results have been compared with finite element analyses. Based on the outcome of this initial evaluation, further refinements in design and manufacturing are proposed.

Introduction.
Calibration of full-field optical deformation measurement systems is an essential step in providing traceability and promoting confidence in relation to displacement and strain distributions obtained from experiment. Calibration is also highly desirable when the full-field experimental data is used to validate computational models employed in engineering design. Therefore, the ADVISE project (Advanced Dynamic Validation through Integration of Simulations and Experimentation) [[1]] has set out to develop a Reference Material (RM) that will allow the calibration of full-field optical systems that are used to capture dynamic deformation fields associated with cyclic and transient loading events. The aim is to design, manufacture and demonstrate a physical RM that generates a known and reproducible displacement/strain field in a defined gauge-zone, as a function of an applied dynamic load. An iterative design process is being followed involving analytical, computational and experimental mechanics techniques in order to reduce possible sources of experimental uncertainty and to simplify the manufacturing process. The first step has been to define and rank desirable attributes of an RM that would facilitate an effective calibration procedure. Then, a set of designs were evaluated to arrive at preferred candidate designs. Subsequently, these designs were elaborated and evaluated further, using CAD and Finite Element Analysis (FEA). Then, prototype RMs were manufactured and experimentally characterised in an inter-lab study using Laser Doppler Velocimetry (LDV) for modal analysis and full-field Digital Speckle Pattern Interferometry (DSPI). This paper summarises the design process employed and the results obtained from this first phase of design evaluation and refinement.

Rational Decision Making Process

The rational decision making model [[2]] was employed to guide the definition and development of the RM, as already done in the design of SPOTS reference material [[3]]. As a first step, a comprehensive set of possible attributes were proposed and used as a basis of an ADVISE questionnaire to engage the engineering community in the weighing of these attributes. The surveyed communities included ADVISE partners and participants of the Society for Experimental Mechanics 2009 Spring Conference (Albuquerque, NM). Contributors were asked to weigh the attributes provided and to propose any extra attributes that they felt should be included. The results of this exercise are shown in Figures 1 and 2, divided into those attributes associated with the displacement field that the RM should generate, and those associated with the general embodiment of the RM.

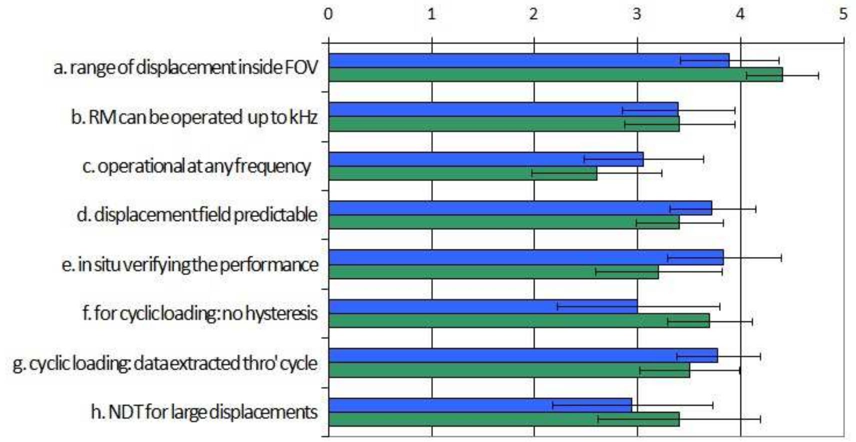

Fig. 1. Attributes and their weightings for the displacement field in the dynamic reference material. (1 - unimportant, 2 - preferred, 3 - important, 4 - highly desirable, or 5 – essential). Green bars denote the ADVISE community whereas the blue bars denote the SEM community.

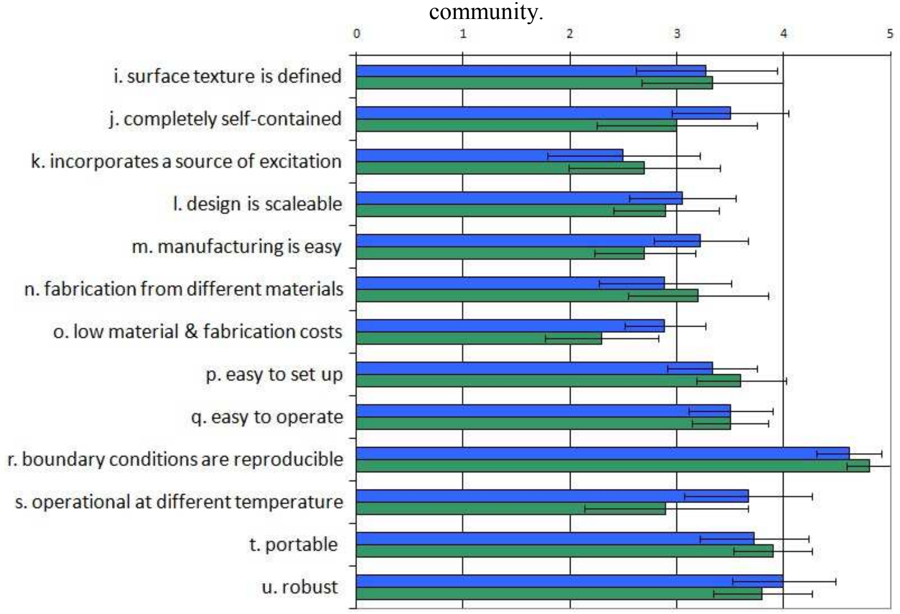

Fig. 2. Attributes and their weightings for the physical embodiment of the dynamic reference material. (1 - unimportant, 2 - preferred, 3 - important, 4 - highly desirable, or 5 – essential). Green bars denote the ADVISE community whereas the blue bars denote the SEM community.

The extra attributes suggested during the survey were that i) the displacement field comprise both out-of-plane and in-plane displacement components, ii) the start and end conditions of the calibration process have to be well defined , iii) the magnitude of displacements could be varied and iv) the RM could be manufactured from a viscoelastic material

Selection of Candidate designs.
The weighted attributes formed the basis of a set of design constraints. The next step in the rational decision making model was to put these constraints aside, and to brainstorm the widest set of possible candidate designs conceivable to the ADVISE partners. Subsequently these design concepts were tested against the essential attributes (high weighting), and those designs that did not possess all of these were rejected. As a result of this filtering process, nine quite different candidate designs were left. The designs selected were then evaluated once more, this time against the desirable attributes (medium weighting), which led to the identification of two favoured candidate designs. These are i) a monolithic rectangular plate held by ligaments within a cylindrical (massive) frame and ii) a monolithic cantilever beam connected to a (massive) block support. As demonstrated in earlier work [[4],[5]], the monolithic design ensures a high degree of repeatability and eliminates any slip phenomena due to clamping at boundaries and fixation points. An FEA study (COMSOL Multiphysics) was then undertaken to model the behaviour of the two complete RM structures to understand and optimise their dynamic behaviour, and to finalise design detail and dimensions before prototype manufacture.

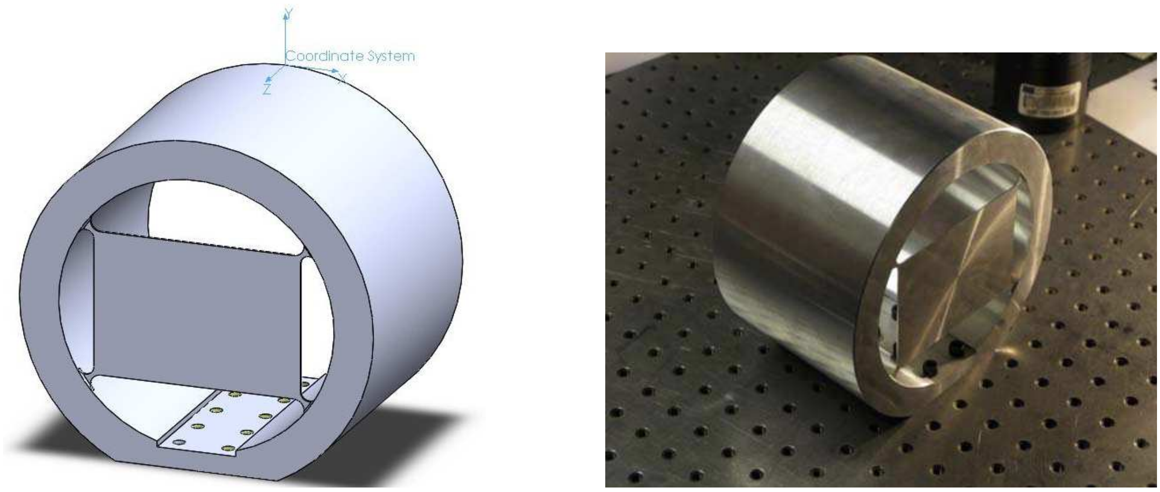

Fig. 3. Rectangular plate RM designed and manufactured for first phase round-robin test.

Evaluation of RM prototype by experimental investigation.
A prototype RM of each design was manufactured. The rectangular plate RM was machined from an extruded round bar of Dural Aluminium, which was turned down inside and out, to produce a stiff cylinder (outer diameter 180 mm) with a flat thin end-face (1mm thickness) The end-face was then milled to produce the plate and the ligaments which attach it to the cylindrical frame (Figure 3). This RM was then evaluated experimentally in an inter-lab study using LDV-based modal analysis and full-field DSPI. A number of excitation sources were investigated including an impact-hammer, electromechanical shaker, sound emitted from a loudspeaker, and a piezoelectric actuator. The restraint conditions applied to the cylindrical frame were also varied, including a simply supported configuration where the RM stayed in position due to its own weight and the flat machined on the outer face of the cylindrical frame (Figure. 3), and a clamped configuration where bolts were used to rigidly attach the RM to a massive base via the flat on the cylindrical frame.
A displacement-based Fast Fourier Transform (FFT) analysis was then carried out using a single-point LDV (Polytec, Germany, model OFV-302) and a dual-channel spectrum analyzer (Bruel & Kiaer) to measure the response over a grid of surface points on the plate. For these initial tests, the RM was clamped by its frame to a rigid optical table. As a first step, impact excitation was used to identify approximately the resonant frequencies, as illustrated in Fig. 5.

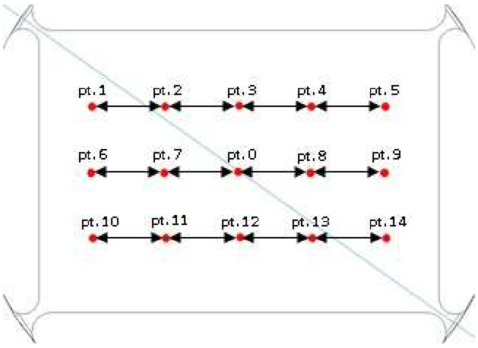

Fig. 4 Plate measurement points

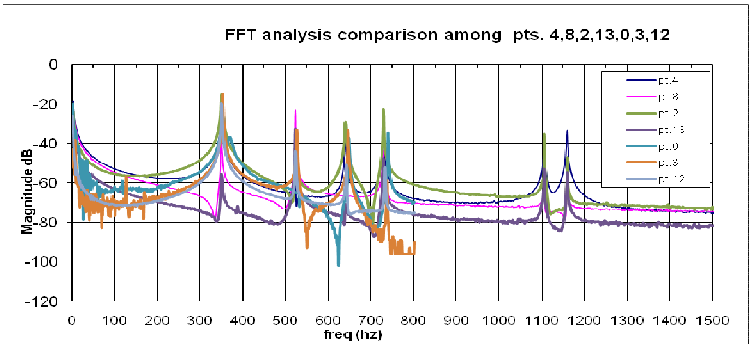

Fig. 5 FFT analysis results by impact excitation on plate RM

The impact excitation was then followed by sine-sweep acoustic excitation to more accurately characterise the resonance behaviour of the plate, as shown in Fig. 5 for some of the analysis points.

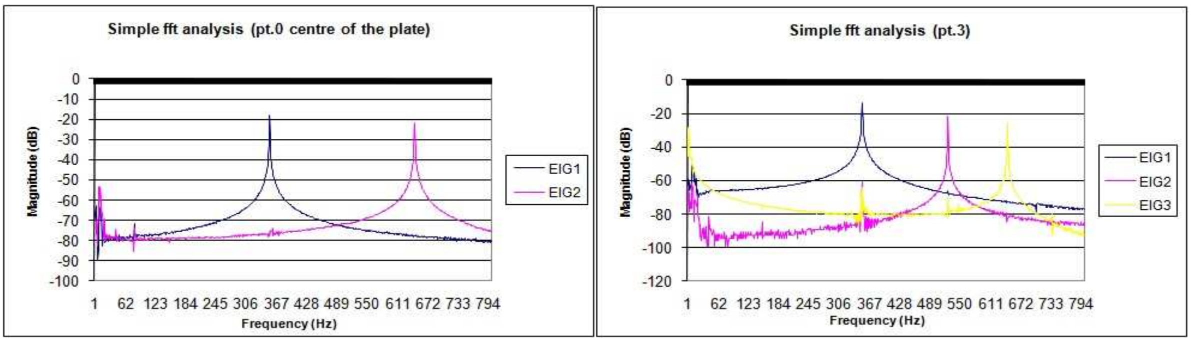

Fig. 6. FFT analysis conducted on RM plate by acoustic excitation

The results obtained by this simple FFT analysis demonstrated the presence of many distinct modal frequencies and a good degree of mode-shape symmetry. Both the experimental and FEA studies indicated a total of twelve resonant frequencies in the range 0 to 2.6 kHz. The experimental modal analysis was extended by mounting the RM on a large electromechanical shaker using a specially designed mounting fixture to orientate the plate horizontally and apply the displacement to the whole RM vertically along its axis. The same LDV instrument was employed to measure the surface vibrations.

Table 1. Plate RM preliminary modal testing results- comparison of Eigen frequencies

modal testing			**FE model (rectangular plate without massive frame)**				
				Pin		Clamp	
mode	Hz		**mode**	Hz	%err	Hz	%err
1	339.0		**1**	200.2	41	268.8	21
2	510.0		**2**	454.9	11	542.3	-6
3	631.2		**4**	679.4	-8	830.0	-31
4	719.8		**3**	541.7	25	669.1	7
5	1081.3		**6**	1250.0	-16	1403.3	-30
6	1144.1		**5**	1136.1	1	1299.2	-14
7	1630.2		**7**	1444.5	11	1524.0	7

The resonant frequencies measured in this shaker configuration are indicated in Table 1, together with the frequencies derived from FEA of an equivalent plate both the case of pin-support at its corners and for the case of clamping around its edges. The classical experimental modal analysis was followed by a full-field study of the RM plate vibration using DSPI. Two different excitation sources were investigated, namely, a loud speaker and a piezoelectric (PZT) actuator, and the RM was tested in both a clamped and unclamped configuration. The first four measured mode shapes and associated resonance frequencies are provided in Fig. 7, for the unclamped configuration, together with the results of FEA where the complete RM was modelled. Out-of-plane displacement field is considered to compare the mode shapes symmetry and difference between DSPI and FEA.

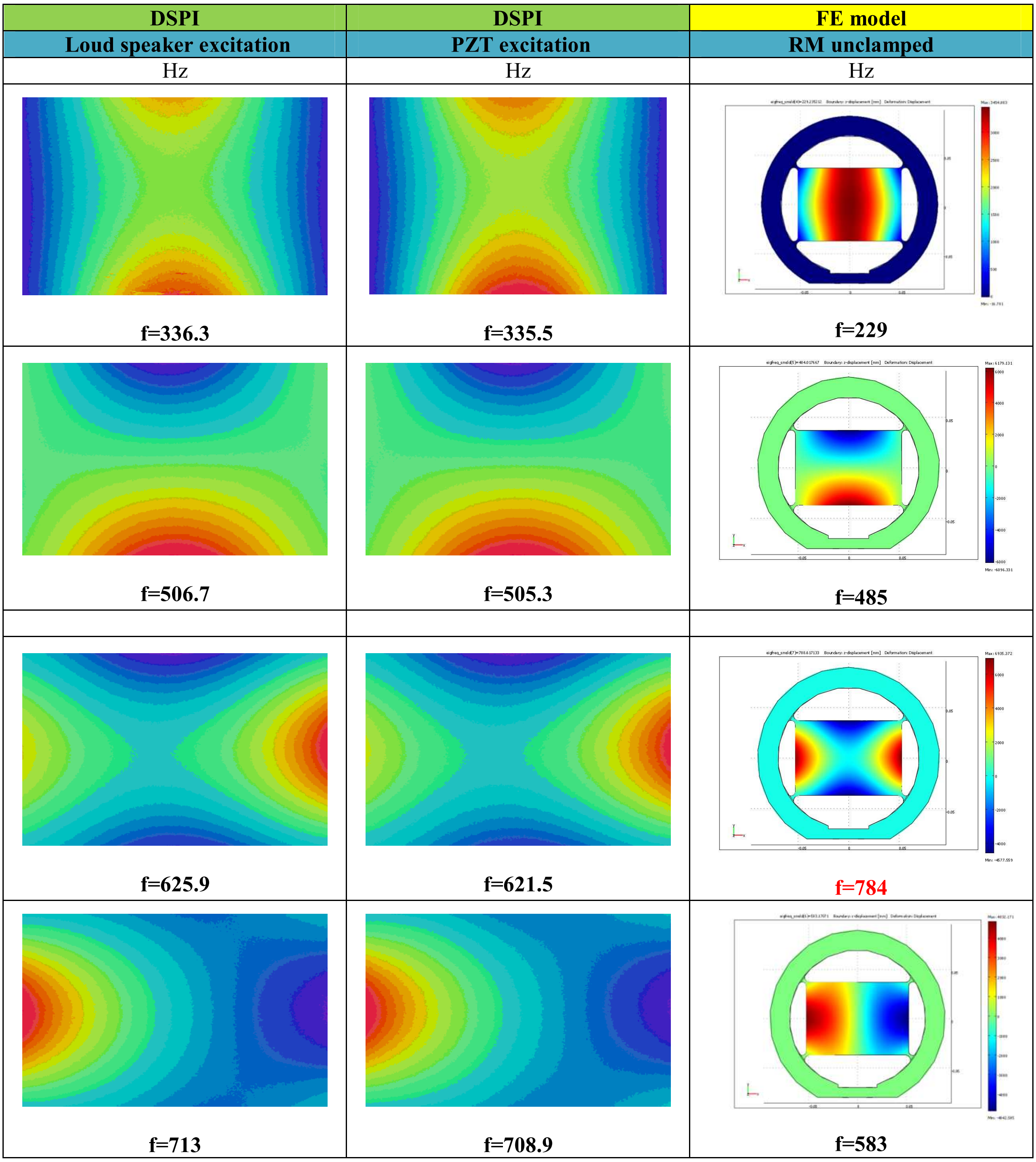

Fig. 7. Comparison between DSPI measurements and FEA for unclamped RM excited by loud speaker and PZT-actuator

The results of the experimental modal analyses and FEA compare quite well. However it can be seen that the position of the third and fourth mode shapes are reversed between experiment and FEA. The modal shapes were quite symmetric for the most part and more so for acoustic excitation when compared to PZT excitation. There was an appreciable gap between experimental and FEA derived resonant frequencies which was surprising considering the rather simple geometry of the RM. A number of explanations were considered for this mismatch in resonant frequencies including dimensional differences between design and prototype, residual stress, flatness of the plate, contributions from the cylindrical frame, and non-linear behaviour of the retaining ligaments. After further investigation through both FEA and experiment, it was concluded that the primary source of discrepancy between the measured and predicted behaviour was due to the residual stress in the RM that remained after manufacture. In addition to this, it was also observed that the cylindrical frame did not behave as a rigid body as was desired, but had a tendency to deform depending on the